Filter Design for a Integrated Non-Isolated AC-Charger

Design of a System Solution with an Integrated AC-Charger Based on the Motor Drive

Electric Power Engineering

YICONG CHEN

MASTER'S THESIS 2018

Redesign and Simulation of the Charging System

Design of a System Solution with an Integrated AC-Charger Based on the Motor Drive

YICONG CHEN

Redesign and Simulation of the Charging System
Design of a System Solution with an Integrated AC-Charger Based on the Motor
Drive
YICONG CHEN

Cover: Volvo 7900 Electric Bus which is Running on Line 55 in Gothenburg

Redesign and Simulation of the Charging System
Design of a System Solution with an Integrated AC-Charger Based on the Motor
Drive
YICONG CHEN
Department of Electrical Engineering
Chalmers University of Technology

Abstract

Electric buses benefit the society both economically and environmentally. Volvo
Group has promoted a Volvo 7900 Electric Bus and it is expected to be able to
carry more passengers and travel a longer distance. To realize that, more batteries
are needed in the bus, which shows the necessity to increase the charging power to
avoid long charging time. Consequently, a charging system with an integrated non-
isolated AC-charger using the existing motor drive as a base is designed, since the
motor drive has higher rated power than the on-board charger being used now. The
simulation is conducted in LTspice, a powerful electrical simulation software. The
intentional and parasitic parameters of all the components in the 600V system are
determined in previous thesis projects[1, 2] and data sheets. One controller of the
motor drive is designed and simulated to manage converting energy from Alternating
Current (AC) to Direct Current (DC) for charging the batteries. In addition, a filter
is also necessary for external requirements from the grid side.

Acknowledgements

This thesis was conducted at Volvo Group in Gothenburg, Sweden between the middle of January and the end of June in 2018.

I would first like to thank my supervisor Mario Salazar Galvez in Volvo Buses, who offered great help throughout the whole process of designing and conducting the master thesis. Being my supervisor since October 2016, Mario has been providing guidance in many aspects during my study in Sweden. He arranged abundant activities for me like workshop and training when I was working on this thesis at Volvo, which enabled me to understand the project better.

In addition, I am grateful to Torbjorn Thiringer, my examiner at Chalmers University of Technology, for his patient work in helping with all my questions and valuable comments on the report. His office is always open when I face some difficulties in the thesis.

Moreover, I would like to express my gratitude to Mats Alakula, Henrik Engdahl, Per Widek and any other colleagues in Volvo Group, who offered great support in their areas during this whole process. This project includes modelling, simulation and so on, which shows a complex work containing different aspects. However, the progress over the past six months was mostly smooth with their assistance of providing technical support and suggestions in every step.

Finally, I must show my gratitude towards my parents for providing me with strong faith and support throughout my study, research and writing this thesis. I could never manage to accomplish all these without them.

<div align="right">Yicong Chen, Gothenburg, June 2018</div>

Contents

List of Abbreviations

AC Alternating Current

CMSB Charger/Motor Switch Box
CSU Charger Switch Unit

DC Direct Current
DCDC DC/DC Converter from 600V System to 24V System
DUT Device under Test

EM Electric Machine
EMD Electric Motor Drive
EMF Electromotive Force
ESS Energy Storage System
EU European Union

FFT Fast Fourier Transform

HEV Hybrid Electric Vehicle
HJB HEV Junction Box
HPC High Power Charging
HVAC Heat, Ventilation and Air Condition

IM Induction Machine

LPC Low Power Charging

OnBC Onboard Charger

PEC Power Electronic Converter
PMSM Permanent Magnet Synchronous Machine
PWM Pulse Width Modulation

THD Total Harmonic Distortion
TVS Traction Voltage System

List of Abbreviations

x

1

Introduction

1.1 Background

Global warming and air pollution have become main environmental problems in the world. To solve these problems, the European Union (EU) countries have achieved an agreement on a new 2030 Framework for climate and energy. Before 2030, the EU will cut down 40% in greenhouse gas emissions compared to the 1990 level. At least a 27% share of renewable energy consumption and 27% energy savings compared with the business-as-usual scenario are also set as targets[3]. It is known to all that the transportation is one of the main reasons why the air pollution and the greenhouse gas emission are heavy[4]. To alter this situation, it is necessary to develop more environmental-friendly modes of transportation, such as hybrid, electric hybrid and full electric buses.

Volvo Buses has promoted several types of Hybrid Electric Vehicles (HEVs) to public, among which the Volvo 7900 Electric Bus needs to be highlighted. The Volvo 7900 Electric Bus which is running on Line 55 in Gothenburg, operates purely on electricity. Since the majority of electricity in Sweden is generated by hydro power plants or nuclear power plants, this bus could almost be viewed as a zero emission vehicle. With regeneration during the braking, the energy consumption can be reduced as well. On the other hand, it also ensures a quiet and comfortable environment for both passengers and drivers.

The Traction Voltage System (TVS) is the main system that stores electric energy and supplies power to the vehicle. The Onboard Charger (OnBC) and the Electric Motor Drive (EMD) are two important devices in this system, and both of them are Power Electronic Converters (PECs) converting energy between 400VAC and 600VDC. The difference is that the OnBC works as a rectifier to charge the batteries, while the EMD operates as an inverter to drive the traction motor. So, the function of the OnBC can be integrated into the EMD, which means using the EMD also as a non-isolated AC-charger. By doing so, it is possible to raise the charging power since the rated power of the EMD is higher than that of the OnBC. When the charging power becomes higher, the charging time can be shortened, making it possible to increase the rated power of the electric bus and the capacity of batteries in it. As a result, the electric bus would be able to carry more passengers or travel a longer distance within one charge.

1.2   Aim

The aim of this thesis project is to investigate how to design a system solution with an integrated AC-charger using the existing EMD as a base. In particular, the design of a filter is to be investigated in order to fulfill external grid requirements.

1.3   Scope

The first part of this thesis project is the modelling of all main intentional and parasitic components of the vehicle needed in the non-isolated integrated charging solution. An equivalent electrical model will be established to represent all other operational components in the TVS when charging the batteries except for the EMD. Since the main focus is to realize the usage of the EMD as an AC-charger, the model of it should be very detailed, including the controller. Values of all the components are acquired from previous thesis projects[1, 2] and data sheets, since it is outside the time limit to open each device and measure on every component.

Moreover, the design of additional system components is also included, such as a switch box and a filter. The switch box is a group of contactors connected to the AC side of the EMD, switching between the traction motor and the power grid. The filter is placed between the EMD and the power grid to reduce the harmonics in the current and minimize the influence on the grid.

The last part is to run system simulations to evaluate whether the performance of this charging solution outperforms that of the original charging solution using the OnBC. To have an easy start, the equivalent electrical model mentioned above can be replaced with a simple battery model at the beginning. After getting the whole system to operate normally, the equivalent electrical model can be improved to have higher accuracy and stronger adaptability to different vehicles.

1.4   Ethics and Sustainability

In this project, some benefits in sustainability and economy need to be highlighted when conducting it. As an important device in the electric bus, the integrated non-isolated AC-charger based on the motor drive will not affect either the consumer or the operator in the workshop. This is because this change happens inside the vehicle. Integrating the function of the original OnBC into the EMD enables the company to develop the next generation of electric buses which can carry more passengers and travel longer distance. This will benefits the environment. Meanwhile, this improvement will save the cost for the manufacture and could decrease the price of the electric bus. It will strengthen the enthusiasm of governments to develop the public transportation instead of private vehicles and benefit the economy as well.
In the long run, this thesis has a considerable amount of societal advantages in different aspects. Although, the influence on the power grid and other performances of the

vehicle after utilizing this integrated non-isolated AC-charger wait to be discussed in the procedure.

1.5 Limitations

The first limitation is that electrical models of all the devices are acquired from previous projects due to that almost all the components in each device cannot be fetched out for measurement. Meanwhile, all the devices containing PECs except for the EMD are simplified by only keeping devices on the DC side because they will be the only connected parts when the PECs in those devices are not operational.

In addition, the cable connecting the EMD and the traction motor is not considered in the simulation, neither is the switch box. It is because their layout have not been decided yet and they do not have much influence on simulation results. The power grid in the simulation model is assumed to be a strong grid with zero grid inductance, but the value of the grid inductance could vary depending on the actual position of the charging station. These limitations all affect the accuracy of the system and could be improved in a future work.

1.6 Outline

Chapter 1 introduces the motivation for this project and the benefits it could bring. A brief description of the work content is also included in this chapter. Chapter 2 demonstrates all the theoretical knowledge necessary for this project, including the converter, the control strategy of it, the filter design and the inductor design. Chapter 3 focuses on the 600V system in the full electric bus and some important parameters need to be taken care of when redesign it. The challenge in this thesis is also presented. Chapter 4 shows how the simulation model is designed in the simulation software. Chapter 5 presents results of the simulation to see whether an accurate model and a satisfying simulating performance is achieved. Sensitivity analysis and discussions about the solution provided are also included. In Chapter 6, conclusions of this thesis project and a future work is revealed.

2

Theory

2.1 Converters and Voltage Modulation
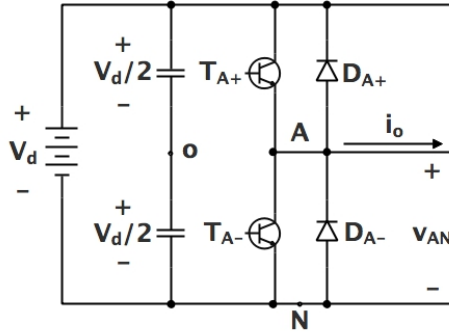
Figure 2.1: One-Leg Switch-Mode Inverter

The AC-charger simulated in this thesis is an inverter which can convert energy from 400VAC to 600VDC. Pulse Width Modulation (PWM) is the most common method to control the output voltage and the power flow of inverters. Viewing a one-leg switch-mode inverter shown in Figure 2.1 as an example, the PWM will be introduced. As can be seen in Figure 2.1, one leg in the inverter consists of two switches. When one switch is in the on state, the other one must be off to prevent from short circuiting the DC voltage source. The output voltage v_{Ao} of a one-leg switch-mode inverter depends on the control signal $v_{control}$ and triangular signal v_{tri}. If $v_{control} > v_{tri}$, the upper switch T_{A+} is turned on and the lower one T_{A-} is off. Consequently, the output voltage v_{Ao} is equal to $+V_d/2$. On the other hand, the output voltage is $-V_d/2$ when T_{A+} is off and T_{A-} is on, once $v_{control} < v_{tri}$. An amplitude modulation ratio m_a is defined as

$$m_a = \frac{\hat{V}_{control}}{\hat{V}_{tri}} \tag{2.1}$$

where $\hat{V}_{control}$ is the peak amplitude of $v_{control}$. The amplitude of v_{tri}, $\hat{V}_{tri}$ is generally kept constant. A frequency modulation ratio m_f is defined as

$$m_f = \frac{f_s}{f_1} \tag{2.2}$$

where f_s is the switching frequency and f_1 is the desired fundamental frequency of the output signal. Figure 2.2(a) presents waveforms of $v_{control}$ and v_{tri}. In this case,
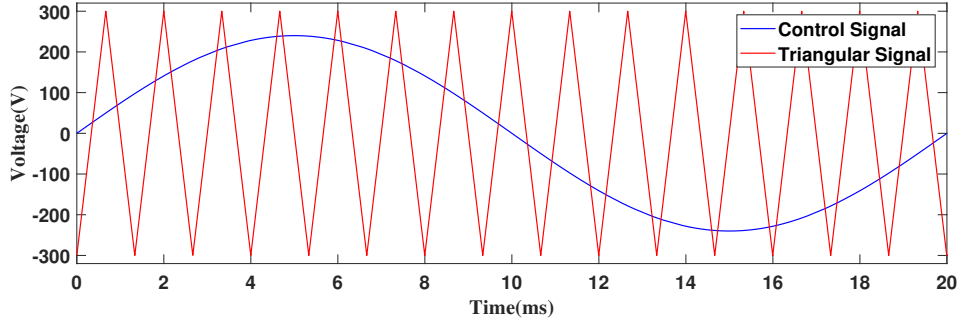
(a) Voltage Modulation
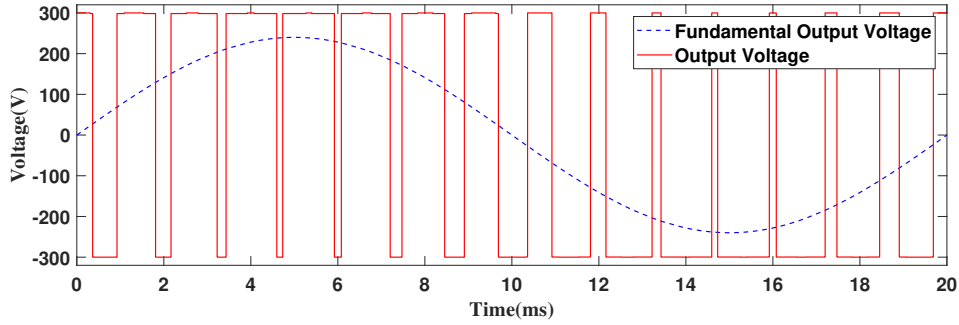
(b) Output Voltage

Figure 2.2: Pulse Width Modulation

$m_a = 0.8$, $m_f = 15$, $f_1 = 50\text{Hz}$ and $V_d = 600\text{V}$. According to the switching strategy previously described, the average output voltage V_{Ao} over one switching period T_s ($T_s = 1/f_s$) is calculated as

$$V_{Ao} = \frac{v_{control}}{\hat{V}_{tri}}\frac{V_d}{2} \qquad v_{control} < \hat{V}_{tri} \tag{2.3}$$

$v_{control}$ is set to be sinusoidal at a frequency of $\omega_1 = 2\pi f_1$ to provide a sinusoidal output voltage with fewer harmonics, i.e.

$$v_{control} = \hat{V}_{control}\sin\omega_1 t \tag{2.4}$$

With (2.3) and (2.4), the fundamental component in v_{Ao} can be expressed to be

$$\begin{aligned}(v_{Ao})_1 &= \frac{\hat{V}_{control}}{\hat{V}_{tri}}\frac{V_d}{2}\sin\omega_1 t \\ &= m_a\frac{V_d}{2}\sin\omega_1 t \qquad m_a \leqslant 1.0\end{aligned} \tag{2.5}$$

Therefore, the magnitude of $(v_{Ao})_1$ is

$$(\hat{V}_{Ao})_1 = m_a\frac{V_d}{2} \qquad m_a \leqslant 1.0 \tag{2.6}$$

which shows that $(\hat{V}_{Ao})_1$ varies linearly with m_a[5]. The waveform of v_{Ao} and $(v_{Ao})_1$ are presented in Figure 2.2(b).

In this project, the EMD is the only PEC that is completely modelled, since it is the most essential component when charging the batteries. In the following subsections, the three-phase inverter and different voltage modulation schemes will be introduced.

2.1.1 Three-Phase Inverter
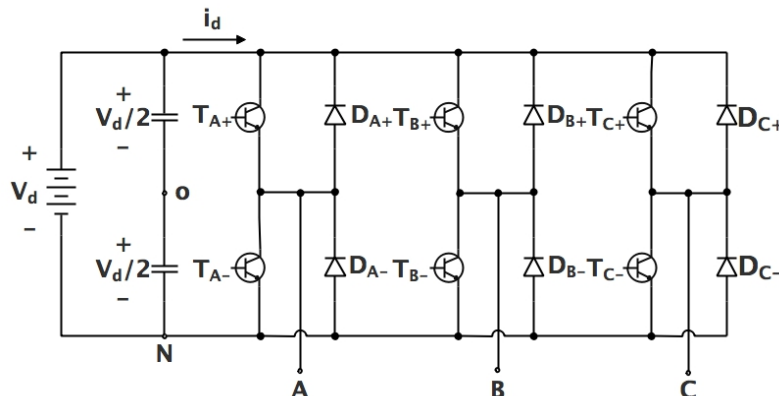
Figure 2.3: Three-Phase Inverter

The most frequently used three-phase inverter circuit consists of three legs as exhibited in Figure 2.3. According to the previous discussion, the output of each leg depends only on V_d and the switch status. The switching strategy of each phase follows the same one applied when controlling the one-leg switch-mode inverter. m_a should be smaller than 1, because only linear modulation will be discussed in this section. The reason for this is that over-modulation will introduce more harmonics into the current[5] which affects the performance of the filter.

Figure 2.4 presents the three-phase PWM and the output voltage[5]. Considering all the parameters to be the same as before ($m_a = 0.8$, $m_f = 15$, $f_1 = 50$Hz and $V_d = 600$V), the waveform can be derived accurately. It can be observed that the peak value of the fundamental component in the phase voltage, for example $(\hat{V}_{AN})_1$ (with respect to the negative DC bus), can be expressed by

$$(\hat{V}_{AN})_1 = m_a \frac{V_d}{2} \tag{2.7}$$

Therefore, the RMS value of the fundamental component in the line voltage, due to the 120° phase displacement between phase voltages, is written as

$$
\begin{aligned}
V_{LL1} &= \frac{\sqrt{3}}{\sqrt{2}}(\hat{V}_{AN})_1 \\
&= \frac{\sqrt{3}}{2\sqrt{2}}m_a V_d \\
&\approx 0.612 m_a V_d \qquad m_a \leqslant 1.0
\end{aligned}
\tag{2.8}
$$
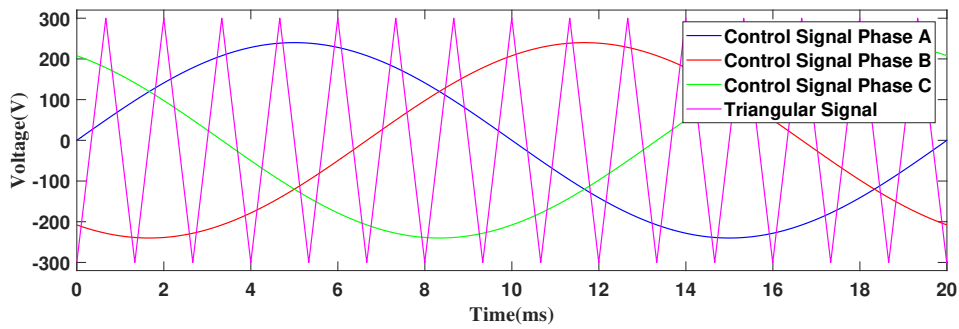
(a) Three-Phase Voltage Modulation
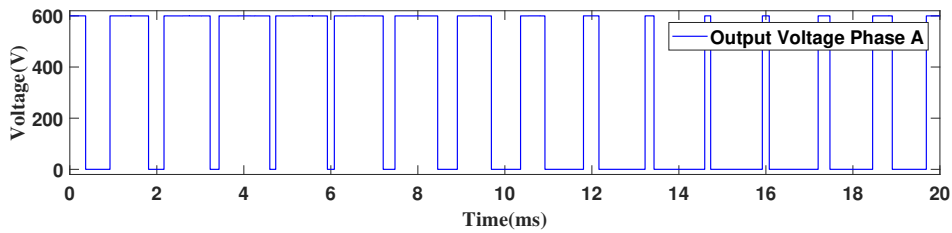
(b) Phase A Voltage
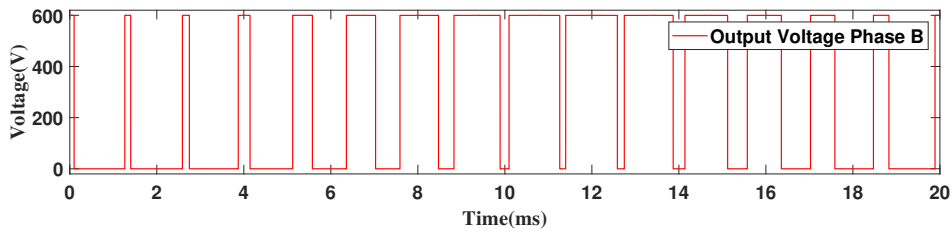
(c) PhaseB Voltage
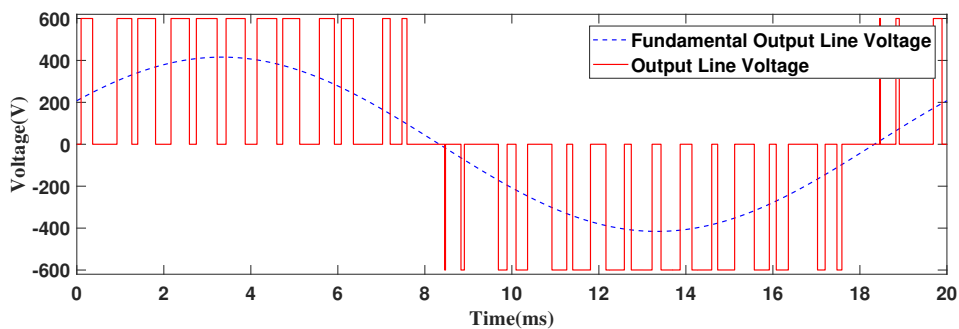
(d) Line Voltage

Figure 2.4: Three-Phase PWM

2.1.2 Modulation Schemes

The PWM modulation presented in Figure 2.4(a) shows the sinusoidal modulation. Besides, two other common modulation schemes are symmetrical modulation and bus-clamped modulation. The only difference among these modulation schemes for three-phase converters is the voltage reference waveform. More accurately, the

difference is whether a zero-sequence signal is added to the control signal and what the zero sequence signal is like if it is needed[6]. A zero-sequence signal in the voltage reference waveform will not show up in the output voltage because the connected machine is not connected to the neutral. Consequently, the converter is not able to influence the neutral voltage. A zero-sequence phase voltage results in a zero-sequence current while the zero-sequence current has no path to flow through[7]. The voltage reference waveforms for different modulation schemes are shown in Figure 2.5.
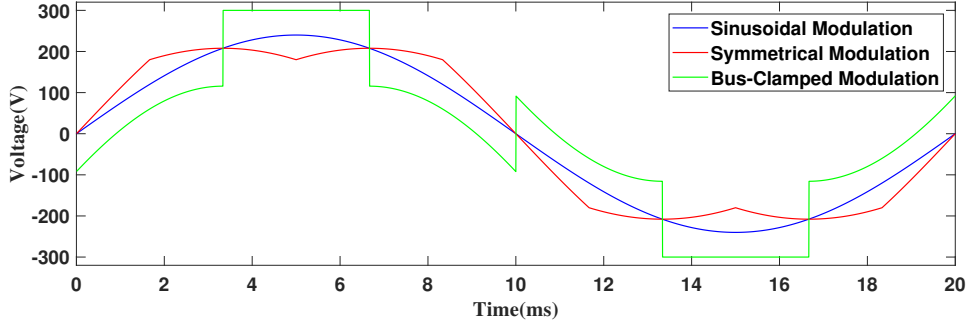
Figure 2.5: Voltage References for the Different Modulation Schemes

It can be seen that for the sinusoidal modulation, the voltage reference waveform is kept as a sinusoidal phase voltage. For the symmetrical modulation, the most positive and the most negative voltage reference waveforms are made to be equal but with opposite signs. For the bus-clamped modulation, the phase voltage reference waveform with the highest instantaneous absolute value is clamped to $\pm V_d/2$ which depends on its polarity.

From (2.12), the maximum RMS value of the line voltage for the sinusoidal modulation is achieved when $m_a = 1.0$, which is

$$V_{LL1,\max} = 0.612V_d \tag{2.9}$$

For the symmetrical modulation, the zero-sequence signal and the resulting voltage reference are calculated as

$$u_z = \frac{1}{2}[\max(u_{a,ref}, u_{b,ref}, u_{c,ref}) + \min(u_{a,ref}, u_{b,ref}, u_{c,ref})]$$
$$u_{iz,ref} = u_{i,ref} - u_z \qquad i = a, b, c \tag{2.10}$$

For $1/6^{th}$ of the fundamental period when $u_{a,ref}$ is the most positive phase voltage reference waveform and $u_{b,ref}$ is the most negative one, the resulting voltage reference for phase A is written as

$$u_{a,ref} = \hat{V}_{control} \sin \omega_1 t$$
$$u_{b,ref} = \hat{V}_{control} \sin (\omega_1 t - 120°)$$
$$u_z = \frac{1}{2}(u_{a,ref} + u_{b,ref}) = \frac{1}{2}\hat{V}_{control} \sin (\omega_1 t - 60°) \tag{2.11}$$
$$u_{az,ref} = u_{a,ref} - u_z = \frac{\sqrt{3}}{2}\hat{V}_{control} \sin (\omega_1 t + 30°) \qquad \omega_1 t \in [30°, 90°]$$

9

The maximum value of the resulting voltage reference $\sqrt{3}\hat{V}_{control}/2$ is obtained at $\omega_1 t = 60°$ and should be limited within $+V_d/2$. Hence, the maximum RMS value of the line voltage for symmetrical modulation is equal to

$$
\begin{aligned}
V_{LL1,\text{max}} &= \frac{\sqrt{3}}{\sqrt{2}}\hat{V}_{control,\text{max}} \\
&= \frac{\sqrt{3}}{\sqrt{2}\sqrt{3}}V_d \\
&\approx 0.707V_d
\end{aligned}
\tag{2.12}
$$

For the bus-clamped modulation, the transition between two bus-clamped references is investigated. Considering the point when the phase A voltage reference has been clamped to $+V_d/2$ and the phase C voltage reference is about to be clamped to $-V_d/2$, the resulting voltage reference for phase A can be calculated as

$$
\begin{aligned}
u_{a,ref} &= \hat{V}_{control} \sin \omega_1 t \\
u_{c,ref} &= \hat{V}_{control} \sin (\omega_1 t + 120°) \\
u_z &= u_{c,ref} - (-\frac{V_d}{2}) = \hat{V}_{control} \sin (\omega_1 t + 120°) + \frac{V_d}{2} \\
u_{az,ref} &= u_{a,ref} - u_z = \sqrt{3}\hat{V}_{control} \sin (\omega_1 t - 30°) - \frac{V_d}{2} \qquad \omega_1 t \in [120°, 180°]
\end{aligned}
\tag{2.13}
$$

The maximum value of the resulting voltage reference $\sqrt{3}\hat{V}_{control} - V_d/2$ is obtained at $\omega_1 t = 120°$ and should be limited within $+V_d/2$. Therefore, the maximum RMS value of line voltage for the bus-clamped modulation is

$$
\begin{aligned}
V_{LL1,\text{max}} &= \frac{\sqrt{3}}{\sqrt{2}}\hat{V}_{control,\text{max}} \\
&= \frac{\sqrt{3}}{\sqrt{2}\sqrt{3}}(\frac{V_d}{2} + \frac{V_d}{2}) \\
&\approx 0.707V_d
\end{aligned}
\tag{2.14}
$$

In conclusion, both the symmetrical modulation and the bus-clamped modulation provide a 15% higher margin to the over-modulation compared to the sinusoidal modulation. The symmetrical modulation has less current ripple than the bus-clamped modulation[7]. However, the bus-clamped modulation will reduce the number of commutations and the switching loss[8]. However, since reducing the switching loss can also be realized through choosing lower switching frequency, the symmetrical modulation is more widely utilized.

2.2 Filter

The requirement for high frequency harmonics in the line current on the grid side when charging is described in the regulation[9], which makes a filter necessary for this system as shown in Figure 3.3. The harmonics are created by the switched

operation of the three-phase inverter and an LCL-filter shown in Figure 2.6 can be utilized in this case.
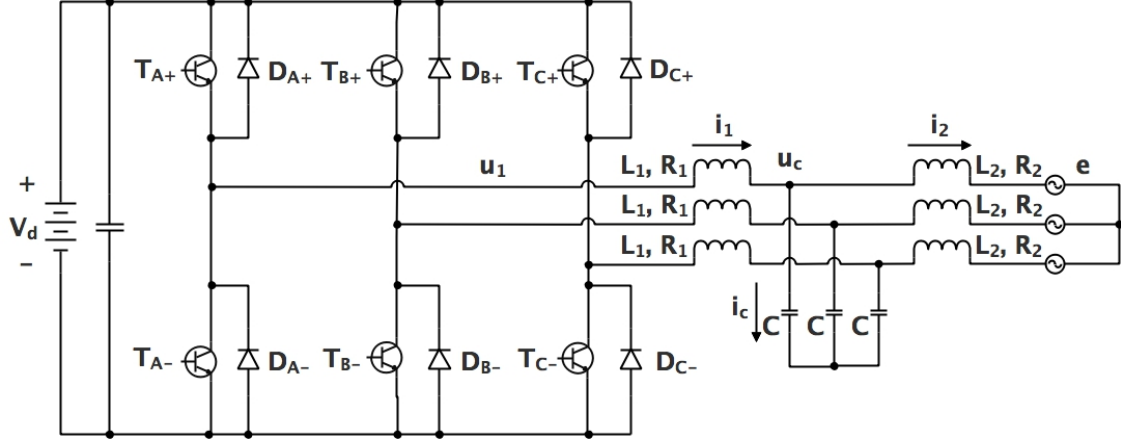
Figure 2.6: Line Side of the Inverter with the LCL-Filter

The differential equations of the LCL-filter in the stationary $\alpha\beta$-frame are

$$
\begin{aligned}
\frac{d}{dt}\vec{i}_1^{\alpha\beta} &= -\frac{R_1}{L_1}\vec{i}_1^{\alpha\beta} + \frac{1}{L_1}(\vec{u}_1^{\alpha\beta} - \vec{u}_c^{\alpha\beta}) \\
\frac{d}{dt}\vec{u}_c^{\alpha\beta} &= \frac{1}{C}(\vec{i}_1^{\alpha\beta} - \vec{i}_2^{\alpha\beta}) \\
\frac{d}{dt}\vec{i}_2^{\alpha\beta} &= -\frac{R_2}{L_2}\vec{i}_2^{\alpha\beta} + \frac{1}{L_2}(\vec{u}_c^{\alpha\beta} - \vec{e}^{\alpha\beta})
\end{aligned}
\tag{2.15}
$$

which are equally presented in the format of matrix

$$
\frac{d}{dt}
\begin{bmatrix} \vec{i}_1^{\alpha\beta} \\ \vec{u}_c^{\alpha\beta} \\ \vec{i}_2^{\alpha\beta} \end{bmatrix}
=
\underbrace{
\begin{bmatrix}
-\dfrac{R_1}{L_1} & -\dfrac{1}{L_1} & 0 \\
\dfrac{1}{C} & 0 & -\dfrac{1}{C} \\
0 & \dfrac{1}{L_2} & -\dfrac{R_2}{L_2}
\end{bmatrix}}_{\boldsymbol{A}_{LCL}^{\alpha\beta}}
\begin{bmatrix} \vec{i}_1^{\alpha\beta} \\ \vec{u}_c^{\alpha\beta} \\ \vec{i}_2^{\alpha\beta} \end{bmatrix}
+
\underbrace{
\begin{bmatrix}
\dfrac{1}{L_1} & 0 \\
0 & 0 \\
0 & -\dfrac{1}{L_2}
\end{bmatrix}}_{\boldsymbol{B}_{LCL}^{\alpha\beta}}
\begin{bmatrix} \vec{u}_1^{\alpha\beta} \\ \vec{e}^{\alpha\beta} \end{bmatrix}
\tag{2.16}
$$

To calculate the inductance and the capacitance needed for designing this filter, some simplification is necessary. For example, the resistance will be neglected ($R_1, R_2 = 0$). Meanwhile, it is assumed that no high frequency harmonics exist in the power grid, so $\vec{e}^{\alpha\beta}$ is set to be zero as well. Afterwards, the transfer function $G^{\alpha\beta}(s)$ can be derived. Consequently, the relationship between the converter output voltage and the line current is

$$
G^{\alpha\beta}(s) = \begin{bmatrix} 0 & 0 & 1 \end{bmatrix} (s\boldsymbol{I} - \boldsymbol{A}_{LCL}^{\alpha\beta})^{-1}\boldsymbol{B}_{LCL}^{\alpha\beta}\begin{bmatrix} 1 \\ 0 \end{bmatrix} = \frac{\dfrac{1}{L_1 L_2 C}}{s\left(s^2 + \dfrac{L_1 + L_2}{L_1 L_2 C}\right)}
\tag{2.17}
$$

11

in which s represents the Laplace operator. The amplitude of this function, replacing ω with $h\omega_1$, can be expressed by

$$\left|G^{\alpha\beta}(jh\omega_1)\right| = \frac{\dfrac{1}{L_1 L_2 C}}{h\omega_1 \left|-h^2\omega_1^2 + \dfrac{L_1 + L_2}{L_1 L_2 C}\right|} \tag{2.18}$$

where h means the order of harmonic and ω_1 is the fundamental angular frequency of the power grid ($f_1 = 50\text{Hz}, \omega_1 = 2\pi f_1$).

To decide these parameters, the ratio between the inner and outer inductors, as well as the idle production of the reactive power by the filter are needed. The ratio between the inductors is associated with the balance between a low resonance frequency and a low current ripple in the inner inductor L_1 and it is suggested to have an inner inductor twice the size of the outer one[10]. Furthermore, it is acceptable that the reactive current injected from the filter is 5% of the nominal line current[11]. Hence, the additional requirements are

$$\begin{aligned} L_1 &= 2L_2 \\ C &= 0.05C_{base} \end{aligned} \tag{2.19}$$

where C_{base} is defined as

$$C_{base} = \frac{1}{\omega_{base} Z_{base}} = \frac{I_{base}}{\omega_1 U_{base}} = \frac{\sqrt{3}I_N}{\omega_1 U_N} \tag{2.20}$$

which U_N is the RMS value of the line voltage of the grid and I_N is the rated line current. With these additional requirements, the outer inductor L_2 can be calculated as

$$L_2 = \max_h \left(\frac{3}{4Ch^2\omega_1^2} + \sqrt{\left(\frac{3}{4Ch^2\omega_1^2}\right)^2 + \frac{U_{phase,h}}{2Ch^3\omega_1^3 I_{h,\max}}} \right) \tag{2.21}$$

where $U_{phase,h}$ refers to the RMS value of the hth order harmonic in the output phase voltage and $I_{h\max}$ is the maximum value of the hth order harmonic in the line current.

As a simple solution, an L-filter is also feasible in this case. The design of an L-filter can be observed in Figure 2.7. The differential equation of the L-filter is described as

$$\frac{d}{dt}\vec{i}^{\alpha\beta} = -\frac{R}{L}\vec{i}^{\alpha\beta} + \frac{1}{L}(\vec{u}^{\alpha\beta} - \vec{e}^{\alpha\beta}) \tag{2.22}$$

Neglecting the resistance and assuming $\vec{e}^{\alpha\beta}$ only consists of the fundamental component, the transfer function between the converter output voltage and the line current is

$$\begin{aligned} G^{\alpha\beta}(s) &= \frac{1}{sL} \\ \left|G^{\alpha\beta}(jh\omega_1)\right| &= \frac{1}{h\omega_1 L} \end{aligned} \tag{2.23}$$
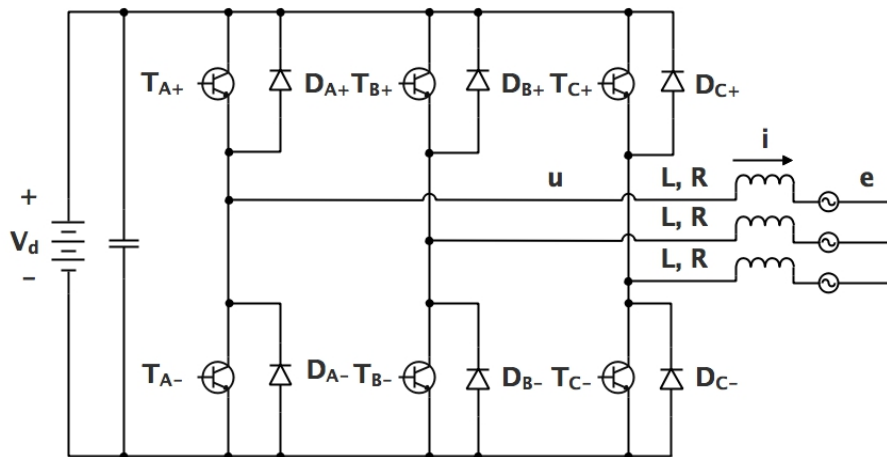
Figure 2.7: Line Side of the Inverter with the L-Filter

As a result, the design expression for the inductor L is given by

$$L = \max_h \left(\frac{U_{phase,h}}{h\omega_1 I_{h\,\max}} \right)$$ (2.24)

2.3 Park's Transformation

Park's Transformation is an approach introduced by R. H. Park in the late 1920s to analyze the electric machines[12]. This approach transforms the stator variables to a rotating reference fixed to the rotor and is able to eliminate all time-varying inductances from the voltage equations of the synchronous machine. Since then, researchers introduced different changes into this approach for a more extensive application scope[13]. The largest advantage of Park's Transformation is its ability to realize current decoupled control of AC electric machines, which highly increases the control performance of AC machines. The Amplitude Invariant Transformation that can convert three-phase stationary variables to the rotating dq-frame is expressed by

$$\begin{aligned}
\boldsymbol{F_{dq0}} &= \boldsymbol{T_A} \boldsymbol{F_{abc}} \\
\boldsymbol{F_{dq0}} &= \begin{bmatrix} f_d & f_q & f_0 \end{bmatrix}^T \\
\boldsymbol{F_{abc}} &= \begin{bmatrix} f_a & f_b & f_c \end{bmatrix}^T \\
\boldsymbol{T_A} &= \frac{2}{3} \begin{bmatrix} \cos\theta & \cos(\theta - \frac{2\pi}{3}) & \cos(\theta + \frac{2\pi}{3}) \\ -\sin\theta & -\sin(\theta - \frac{2\pi}{3}) & -\sin(\theta + \frac{2\pi}{3}) \\ \frac{1}{2} & \frac{1}{2} & \frac{1}{2} \end{bmatrix}
\end{aligned}$$ (2.25)

where θ is the angle difference between the rotating dq-frame and the three-phase stationary frame and it is calculated as

$$\begin{aligned} \theta &= \int \omega_1 dt \\ &= \int_0^T \omega_1 dt + \theta(0) \end{aligned}$$

(2.26)

The coefficient 2/3 keeps the amplitude of the vectors unchanged after the transformation. Meanwhile, the Inverse Amplitude Invariant Transformation is shown as

$$\boldsymbol{T_A^{-1}} = \begin{bmatrix} \cos\theta & -\sin\theta & 1 \\ \cos(\theta - \dfrac{2\pi}{3}) & -\sin(\theta - \dfrac{2\pi}{3}) & 1 \\ \cos(\theta + \dfrac{2\pi}{3}) & -\sin(\theta + \dfrac{2\pi}{3}) & 1 \end{bmatrix}$$

(2.27)

It is also possible to use other coefficients in the transformations. For instance, the Power Invariant Transformation is obtained when the efficient is chosen to be $\sqrt{2/3}$ as presented

$$\boldsymbol{T_P} = \sqrt{\dfrac{2}{3}} \begin{bmatrix} \cos\theta & \cos(\theta - \dfrac{2\pi}{3}) & \cos(\theta + \dfrac{2\pi}{3}) \\ -\sin\theta & -\sin(\theta - \dfrac{2\pi}{3}) & -\sin(\theta + \dfrac{2\pi}{3}) \\ \dfrac{\sqrt{2}}{2} & \dfrac{\sqrt{2}}{2} & \dfrac{\sqrt{2}}{2} \end{bmatrix}$$

(2.28)

and the Inverse Power Invariant Transformation matrix is

$$\boldsymbol{T_P^{-1}} = \begin{bmatrix} \cos\theta & -\sin\theta & \dfrac{\sqrt{2}}{2} \\ \cos(\theta - \dfrac{2\pi}{3}) & -\sin(\theta - \dfrac{2\pi}{3}) & \dfrac{\sqrt{2}}{2} \\ \cos(\theta + \dfrac{2\pi}{3}) & -\sin(\theta + \dfrac{2\pi}{3}) & \dfrac{\sqrt{2}}{2} \end{bmatrix}$$

(2.29)

The Amplitude Invariant Transformation is applied in this thesis. Commonly, the zero component in the dq-frame can be ignored during practical applications. In this project, viewing the grid voltage as the back-Electromotive Force (EMF), Park's Transformation can be applied to control the output voltage of the inverter in the EMD. When an LCL-filter shown in Figure 2.6 is connected between the EMD and

the grid, the equations in the synchronous rotating dq-frame is obtained.

$$\frac{d}{dt}\begin{bmatrix} \vec{i}_1^{dq} \\ \vec{u}_c^{dq} \\ \vec{i}_2^{dq} \end{bmatrix} = \underbrace{\begin{bmatrix} -\dfrac{R_1}{L_1} - j\omega_1 & -\dfrac{1}{L_1} & 0 \\ \dfrac{1}{C} & -j\omega_1 & -\dfrac{1}{C} \\ 0 & \dfrac{1}{L_2} & -\dfrac{R_2}{L_2} - j\omega_1 \end{bmatrix}}_{\boldsymbol{A}_{LCL}^{dq}} \begin{bmatrix} \vec{i}_1^{dq} \\ \vec{u}_c^{dq} \\ \vec{i}_2^{dq} \end{bmatrix}$$

$$+ \underbrace{\begin{bmatrix} \dfrac{1}{L_1} & 0 \\ 0 & 0 \\ 0 & -\dfrac{1}{L_2} \end{bmatrix}}_{\boldsymbol{B}_{LCL}^{dq}} \begin{bmatrix} \vec{u}_1^{dq} \\ \vec{e}^{dq} \end{bmatrix} \tag{2.30}$$

It is known that in steady state, $\vec{i}_1^{dq}$, $\vec{u}_c^{dq}$ and $\vec{i}_2^{dq}$ are invariable vectors in the synchronous rotating dq-frame, which implies that $\frac{d}{dt}\vec{i}_1^{dq}, \frac{d}{dt}\vec{u}_c^{dq}, \frac{d}{dt}\vec{i}_2^{dq} = 0$. Hence, the voltage equation is derived as

$$\begin{aligned}
\vec{u}_1^{dq} &= [R_1 + R_2 - \omega_1^2(L_1 R_2 + L_2 R_1)]\vec{i}_2^{dq} \\
&+ j\omega_1[L_1 + L_2 + C(R_1 R_2 - \omega_1^2 L_1 L_2)]\vec{i}_2^{dq} \\
&+ (1 - \omega_1^2 C L_1)\vec{e}^{dq} + j\omega_1 C R_1 \vec{e}^{dq}
\end{aligned} \tag{2.31}$$

Separating the d-axis component and the q-axis component, the voltage equations are expressed as

$$\begin{aligned}
u_{1d} &= [R_1 + R_2 - \omega_1^2(L_1 R_2 + L_2 R_1)]i_{2d} \\
&- \omega_1[L_1 + L_2 + C(R_1 R_2 - \omega_1^2 L_1 L_2)]i_{2q} \\
&+ (1 - \omega_1^2 C L_1)e_d - \omega_1 C R_1 e_q \\
u_{1q} &= [R_1 + R_2 - \omega_1^2(L_1 R_2 + L_2 R_1)]i_{2q} \\
&+ \omega_1[L_1 + L_2 + C(R_1 R_2 - \omega_1^2 L_1 L_2)]i_{2d} \\
&+ (1 - \omega_1^2 C L_1)e_q + \omega_1 C R_1 e_d
\end{aligned} \tag{2.32}$$

Similarly, when using an L-filter exhibited in Figure 2.7, the voltage equations are described by

$$\begin{aligned}
\vec{u}^{dq} &= R\vec{i}^{dq} + j\omega_1 L\vec{i}^{dq} + \vec{e}^{dq} \\
u_d &= Ri_d - \omega_1 L i_q + e_d \\
u_q &= Ri_q + \omega_1 L i_d + e_q
\end{aligned} \tag{2.33}$$

2.4 Inductor Design

Since inductors take the majority of the weight of the filter because of the core inside, the weight of them also need to be evaluated in the filter design. The method of calculating the weight of the inductor is presented in this section.
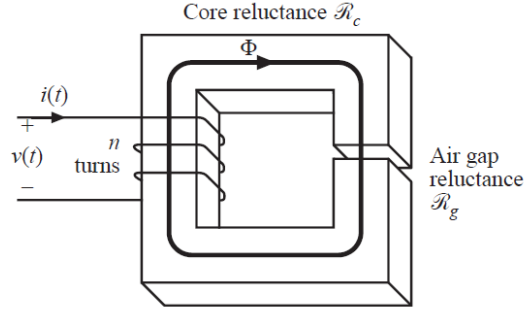
Figure 2.8: Assumed Filter Inductor Geometry

The filter inductor geometry is assumed to be what is shown in Figure 2.8. The air gap is aimed to avoid saturation of the core. The core reluctance R_c is equal to

$$R_c = \frac{l_c}{\mu_c A_c} \tag{2.34}$$

and the air gap reluctance R_g is calculated as

$$R_g = \frac{l_g}{\mu_0 A_c} \tag{2.35}$$

The total magnetic reluctance R is equal to the sum of these two values, so the equivalent permeability μ is derived as

$$R = R_c + R_g = \frac{l_c}{\mu_c A_c} + \frac{l_g}{\mu_0 A_c} = \frac{l_c + l_g}{\mu A_c}$$
$$\mu = \frac{\mu_c \mu_0 (l_c + l_g)}{\mu_0 l_c + \mu_c l_g} \tag{2.36}$$

With the total magnetic reluctance, the inductance is obtained as

$$NI = \Phi R = \frac{\Psi}{N} R$$
$$L = \frac{\Psi}{I} = \frac{N^2}{R} \tag{2.37}$$

where N is the number of turns of the coil, I is the current in the coil, Φ is the flux in the core and Ψ represents the flux linkage in the core. With these equations, the inductor can be designed with following steps:
- Determining the rating of the component, voltage, current, frequency and inductance.
- Selecting appropriate core material, geometry and size.
- Selecting appropriate winding parameters: wire type, size, and number of turns.

3

Case Set-up

3.1 Traction Voltage System in the Electric Bus

The TVS is the high voltage system in electric buses. Its function is to store electric energy and supply power to all the devices inside the bus. A simplified schematic of the TVS in a Volvo 7900 Electric Bus is shown in Figure 3.1.
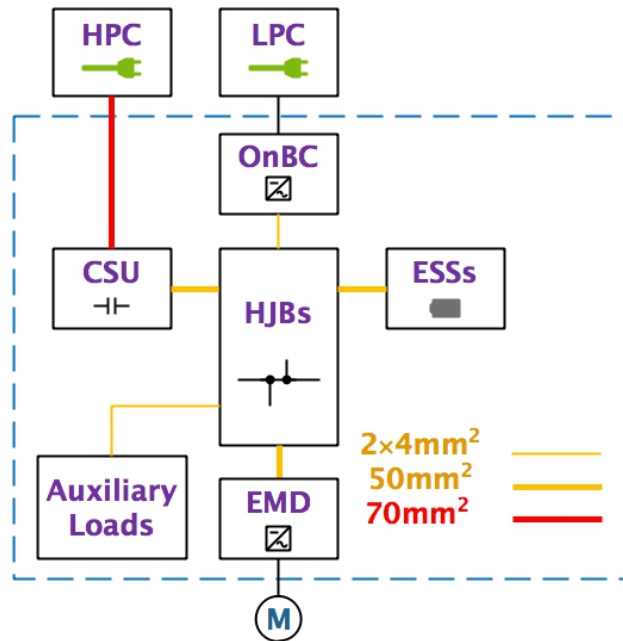
Figure 3.1: Schematic of the TVS in Volvo 7900 Electric Bus

From Figure 3.1, all the important components in the TVS can be observed in the blue dashed lines. The EMD is a PEC that drives the traction motor, which is a Permanent Magnet Synchronous Machine (PMSM). The Energy Storage System (ESS) can be simply viewed as batteries. Since electric buses require more energy from the batteries compared to electric hybrid buses, four ESSs are installed in this system. In an electric hybrid bus, only one ESS is placed in the TVS. The auxiliary loads consists of the Heat, Ventilation and Air Condition (HVAC), the Air Compressor, the DC/DC Converter from 600V System to 24V System (DCDC) and the Auxiliary Heater and they will be elaborated in following sections. The cables with the same potential are connected in the HEV Junction Box (HJB) through metal bars inside.

(a) High Power Charging   (b) Lower Power Charging
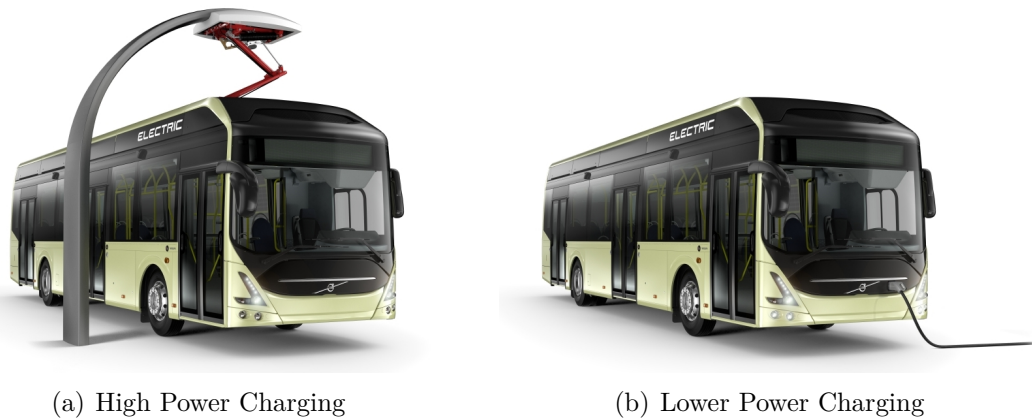
Figure 3.2: Two Charging Schemes for Volvo 7900 Electric Bus

Figure 3.2 demonstrates that two schemes are designed to charge the batteries, which are High Power Charging (HPC) and Low Power Charging (LPC). The HPC shown in Figure 3.2(a) is mounted on the top of the roof. When the bus drives into the charging station, the charger will connect the rails on the top of the bus and charge the batteries with a rated power of 120kW. The LPC which is designed for overnight charging, calibrating and balancing the batteries, is placed at the front of Volvo 7900 Electric Bus as can be seen in Figure 3.2(b). On other vehicles, the position of the OnBC can be the broadside or some other places. The driver will plug the cable into the bus and supply three-phase AC voltage from the grid to the OnBC. The OnBC converts energy from 400VAC to 600VDC with a rated power of 11kW. The Charger Switch Unit (CSU) is like a HJB but with a contactor inside to connect or disconnect the HPC when the bus stays in the charging station.
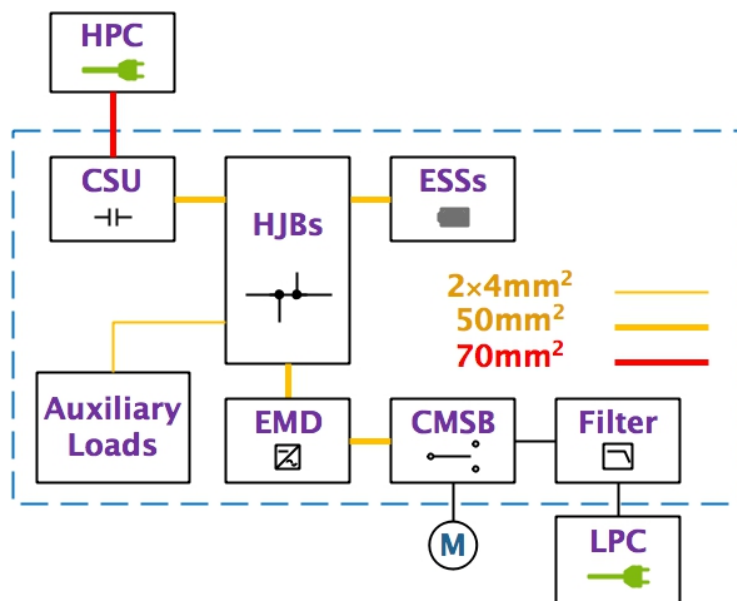
Figure 3.3: New Schematic of the TVS in the Future Electric Bus

A new schematic of the future electric bus can be observed in Figure 3.3 and some

differences need to be highlighted. In this thesis project, the function of the OnBC will be integrated into the EMD. So there will be no OnBC in the new set-up. While charging the bus, the AC side of the EMD will be connected to the power grid through a filter. When driving the bus, it will connect the traction motor. Hence, one additional box containing contactors is needed to switch between the power grid and the traction motor. This box can be named with Charger/Motor Switch Box (CMSB). The filter is aimed to eliminate the high frequency harmonics in the line current on the grid side. Since the HPC and the traction motor is disconnected when conducting overnight charging, it is not necessary to include them in the simulation model for this thesis project. The details of all other devices in the TVS are introduced in subsections.

3.1.1 Electric Motor Drive

The original usage of the EMD is to supply the traction motor with power from the 600V DC side. The Electric Machine (EM) it drives is a PMSM and the base speed of it is reached at a maximum power and a supplied voltage of 600V. The specification values of the EMD are shown in Table 3.1.

Table 3.1: Specification Values of the EMD

Converter Type	Three-Phase Inverter
Switching Frequency	$(f_{sw1}, f_{sw2}, f_{sw3})_{EMD}$
Converter Load Type	PMSM
Converter Load Power	Maximum P_{maxEMD}, Nominal P_{nEMD}
EM Base Speed	n_{EMD}

3.1.2 Heat, Ventilation and Air Condition

The HVAC is a part of the air climate system in the bus. Its operating principle is that one PEC in the HVAC supplies energy to an Induction Machine (IM) which drives a compressor. The specification values of the PEC in the HVAC are found in Table 3.2.

Table 3.2: Specification Values of the Converter in the HVAC

Converter Type	Three-Phase Inverter
Switching Frequency	f_{swHVAC}
Converter Load Type	IM
Converter Load Power	Maximum $P_{maxHVAC}$
EM Base Speed	n_{HVAC}

3.1.3 Air Compressor

The Air Compressor is utilized to provide compressed air to the vehicle. The compressed air is used to operate pneumatic doors on the bus, as well as to brake and

kneel the bus. It is driven by a PMSM and Table 3.3 presents the specification values of the PEC that supplying power to the PMSM.

Table 3.3: Specification Values of the Converter in the Air Compressor

Converter Type	Three-Phase Inverter
Switching Frequency	$f_{swA/C}$
Converter Load Type	PMSM
Converter Load Power	Maximum $P_{maxA/C}$
EM Base Speed	$n_{A/C}$

3.1.4 DC/DC Converter

The DCDC is a PEC that supplies 24VDC to the vehicle used for the steering servo, lights and other auxiliaries. It consists of one full-bridge inverter, one single-phase diode bridge rectifier and one transformer. The specification values of the DCDC can be acquired from Table 3.4.

Table 3.4: Specification Values of the DCDC

Converter Type	Single-Phase DC/DC Converter
Switching Frequency	f_{swDCDC}
Converter Load Type	24VDC System
Converter Load Power	Maximum $P_{maxDCDC}$

3.1.5 Energy Storage System

The ESS is a battery package with coherent subsystems, like the linked controlling system. Four ESSs in total are installed on the top of the roof. The rated voltage of the batteries is 600VDC.

3.1.6 Auxiliary Heater

The Auxiliary Heater is used for heating the passenger compartment. Since there is no combustion engine in the full electric bus, the heater will remedy the deficiency of heat.

3.1.7 Cable

The Volvo 7900 Electric Bus has three types of cables in the TVS differing in their cross section area, which are $2 \times 4\text{mm}^2$, 50mm^2 and 70mm^2. The 70mm^2 cables with a rated current of 195A only connect the rails of the HPC and the CSU. The 50mm^2 ones with a rated current of 155A are used for connection among the traction motor, the EMD, the ESSs, the HJB and the CSU. The remaining parts of the TVS are connected by $2 \times 4\text{mm}^2$ cables, which possess a rated current of 60A. All connections and cable types can be observed in Figure 3.1.

3.2 Grounding Current and Touch Current

The grounding current, also known as leakage current, is the current inside the grounding wire when charging the batteries in the vehicle. The switching of the PEC in the EMD will cause voltage ripple on both the positive and the negative polarities of the DC side. When charging the batteries, the chassis is connected to the ground of the power grid. The voltage change on the two polarities of the DC side will generate current flowing through Y-capacitors and grounding resistors to the ground. It is measured in the grounding resistor (the charging cable in the real application) and it is limited to be 30mA[14].

The touch current is another key indicator needed to be fulfilled when designing the charging system. When there is a grounding fault and one person touches the chassis, the current could flow through human body. The measurement of the touch current is aimed to simulate this situation.

Key
1 connection to electric power supply
2 polarity switch
3 connection of DUT
4 enclosure DUT
5 test probe
6 measurement circuit
7 protective conductor
8 electric power supply
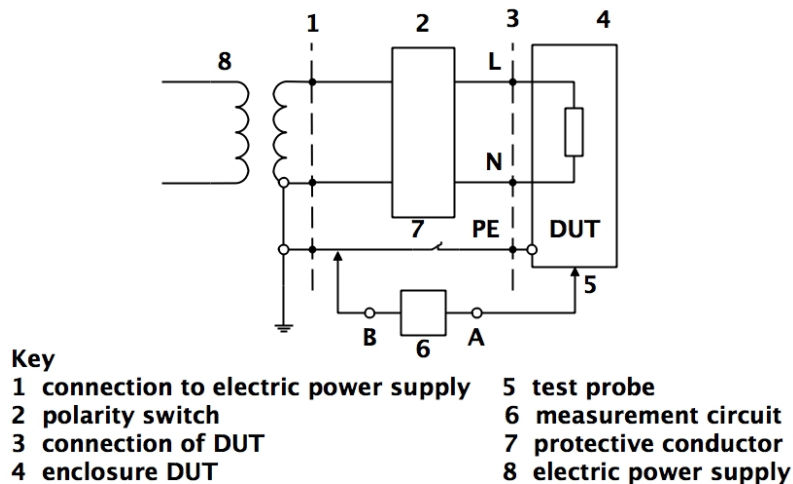
Figure 3.4: Example Test Setup for the Touch Current

The measuring method of the touch current is described in the regulation[15] and shall be measured when the vehicle is connected to an external AC power supply. For the connection between the Device under Test (DUT) and an external power supply with split phase or multiple phases, an appropriate measurement setup needs to be conducted following Figure 3.4. The DUT shall be placed at an isolated position. In case that the conductive parts of the DUT may be live, appropriate safety measurements need to be considered for the testing. The vehicle power supply circuit shall operate at its highest rated power, highest rated frequency and 110% of the highest rated voltage with disconnection of the protective conductor.

The touch current shall then be measured using the measurement circuit referring to Figure 3.5. Terminal B of the measurement circuit is connected to the protective conductor of the measurement setup. Terminal A of the measurement circuit shall be connected to the enclosure of the DUT through a testing probe as can be seen in

Figure 3.4. The measurement shall be performed for the whole surface of the DUT. Nonconductive parts of the enclosure of the DUT shall be covered by a metal foil.

$R_S=1.5\text{k}\Omega\pm5\%$ $R_B=500\Omega\pm5\%$ $R_1=10\text{k}\Omega\pm5\%$
$C_S=0.22\mu\text{F}\pm10\%$ $C_1=0.022\mu\text{F}\pm10\%$
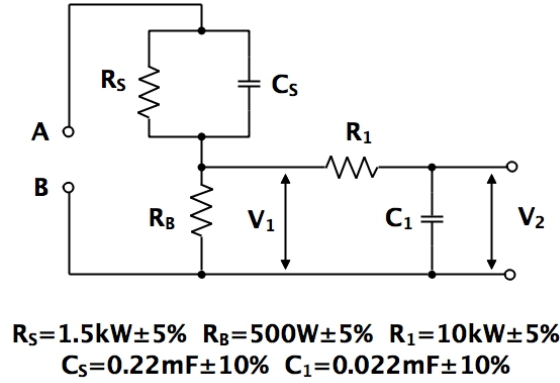
Figure 3.5: Measurement Circuit

The RMS value of the voltage V_2 needs to be measured as presented in Figure 3.5. The instrument used for the voltage measurement shall fulfill the following requirements:
- input resistance $\geqslant 1\text{M}\Omega$
- input capacitance $< 200\text{pF}$
- frequency range 15Hz to 1MHz

The touch current is limited to be within 3.5mA and calculated by[15]

$$I_{RMS} = V_{2RMS}/500 \tag{3.1}$$

3.3   Challenge

The challenge of this thesis mainly comes from limiting the grounding current and the touch current. In the OnBC, a transformer isolate the AC side from the 600V DC side as presented in Figure 3.6. As a result, any other devices in the TVS cannot affect the grid side since there is no direct connection between them. The grounding current of the previous system shown in Figure 3.1 is only generated by the OnBC. However, there is no transformer inside the EMD. Consequently, in the new system as presented in Figure 3.3, all the devices in the TVS will be connected to the ground through the chassis, which puts forward higher requirements for the filter in the new system compared to that in the OnBC. Whether they can reach similar performance and be in a close size will be discussed.
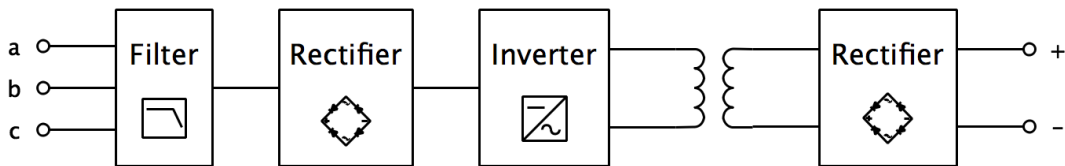
Figure 3.6: Schematic of the OnBC

4

Method

4.1 Simulation Model
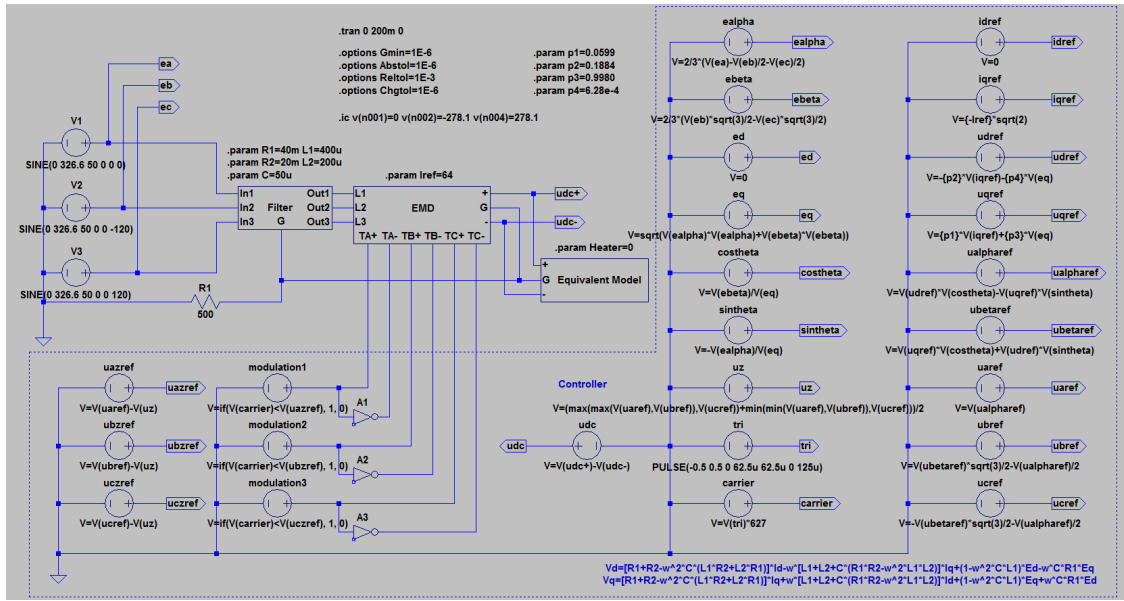
(a) System with the LCL-Filter
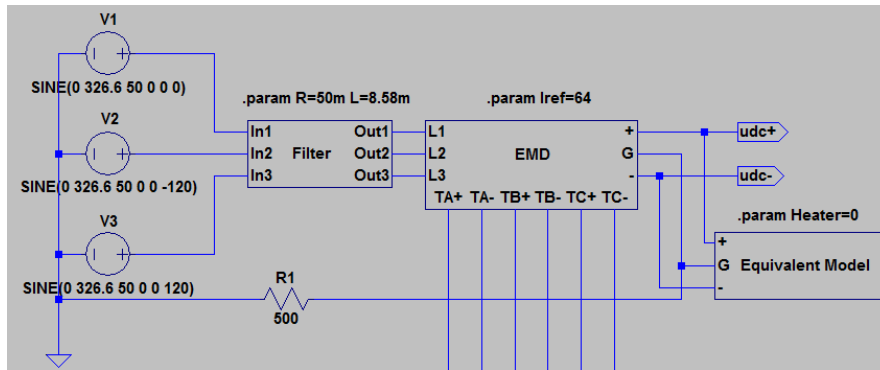
(b) System with the L-Filter
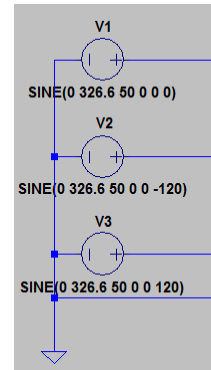
(c) Power Grid

Figure 4.1: Simulation Model of the Charging System

The simulation is conducted in LTspice. Models of the filter and the controller is designed in this thesis, while those of the remaining parts in the TVS are acquired

from previous thesis projects[1, 2] or data sheets. The model of the charging system with the LCL-filter is presented in Figure 4.1(a). The "G" point represents the chassis, which is the common grounding point for all the devices in the TVS. When the system utilize the L-filter, a slight difference can be observed in Figure 4.1(b), which is no connection between the components inside the L-filter and the chassis. The difference will be elaborated in the subsection of the filter. What is exhibited in Figure 4.1(c) is the model of the power grid with a line voltage of 400V and it is assumed to be a strong grid. Consequently, the inductance of the grid is set to be zero. The charging power is restricted by not only the rated power of the EMD, but also limitations in off-board installations, for instance, the current limit of the charging interface at the charging station, cables and connections. Hence, it is selected to be 44kW, which decides the rated line current to be approximately 64A. The HPC is disconnected when charging the batteries from the EMD, so it is not included in this model. Except for that, the other devices are all presented and elaborated in the following sections.

4.2   Filter

(a) LCL-Filter   (b) L-Filter
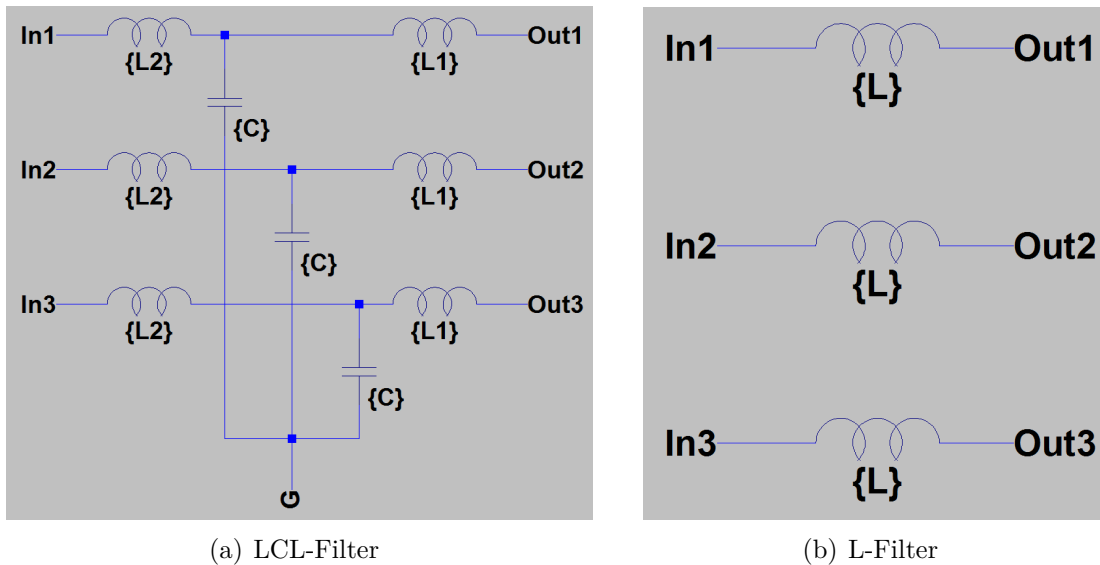
Figure 4.2: Simulation Model of the Filter

The model of the LCL-filter and the L-filter is presented in Figure 4.2. It can be observed that the connection point of Y-connected capacitors in the LCL-filter is grounded. This connection could provide a path for the common mode disturbance to flow through the capacitors back to the system instead of creating large leakage current inside the ground wire.

The simulation is firstly run with only a small inductance ($R = 10\text{m}\Omega, L = 300\mu\text{H}$) on the AC side and the largest harmonic component in the output voltage of the EMD turns out to occur at 8kHz, which is the switching frequency of the EMD.

The RMS value of it is 276V. The expected harmonic current is chosen to be 0.64A which gives a distortion of 1% at this frequency. According to (2.19)∼(2.21), the inductance and the capacitance of the LCL-filter are calculated as

$$C = 0.05C_{base} = 0.05\frac{\sqrt{3}I_N}{\omega_1 U_N} \approx 44.11\mu\text{F} \approx 50\mu\text{F}$$

$$L_2 = \max_h \left(\frac{3}{4Ch^2\omega_1^2} + \sqrt{\left(\frac{3}{4Ch^2\omega_1^2}\right)^2 + \frac{U_{phase,h}}{2Ch^3\omega_1^3 I_{h,\max}}}\right) \tag{4.1}$$

$$\approx 190.30\mu\text{H} \approx 200\mu\text{H}$$

$$L_1 = 2L_2 = 400\mu\text{H}$$

Similarly, based on (2.24), the inductance in the L-filter can be expressed by

$$L = \max_h \left(\frac{U_{phase,h}}{h\omega_1 I_{h\max}}\right) = 8.58\text{mH} \tag{4.2}$$

However, this large inductance would cause over-modulation for the EMD. The method to solve this is described in subsection of the controller. It is also obvious that the LCL-filter can reach the same performance with much smaller inductances, which will take less space.

4.3 Electric Motor Drive
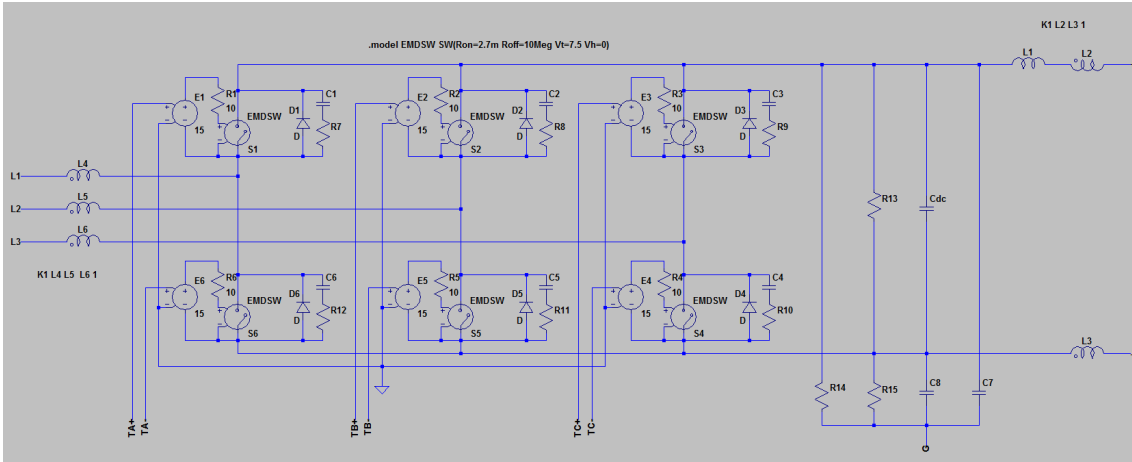
Figure 4.3: Simulation Model of the EMD

The model of the EMD is shown in Figure 4.3 and sketched based on the data sheet. The drive circuit and the switches are ideal models. In the LTspice model, the characteristic of the switch must be defined by an instruction, for example, ".model DSW SW(Ron=2.7m Roff=10Meg Vt=7.5 Vh=0)". It means that the threshold voltage of the switch is 7.5V, and the hysteresis voltage is 0V. The on resistance of the switch is 2.7mΩ and the off resistance is equal to 10MΩ. The inductor group (L2 and L3) described by the LTspice instruction "K1 L2 L3 1" represents a common

mode choke and "1" means that the coefficient of coupling is equal to 1. Besides, it can be seen that the inductor group (L4, L5 and L6) is a common choke as well. The value of L1 is obtained by measurements.

4.4 Controller of the EMD

(a)

(b)

(c)

(d)
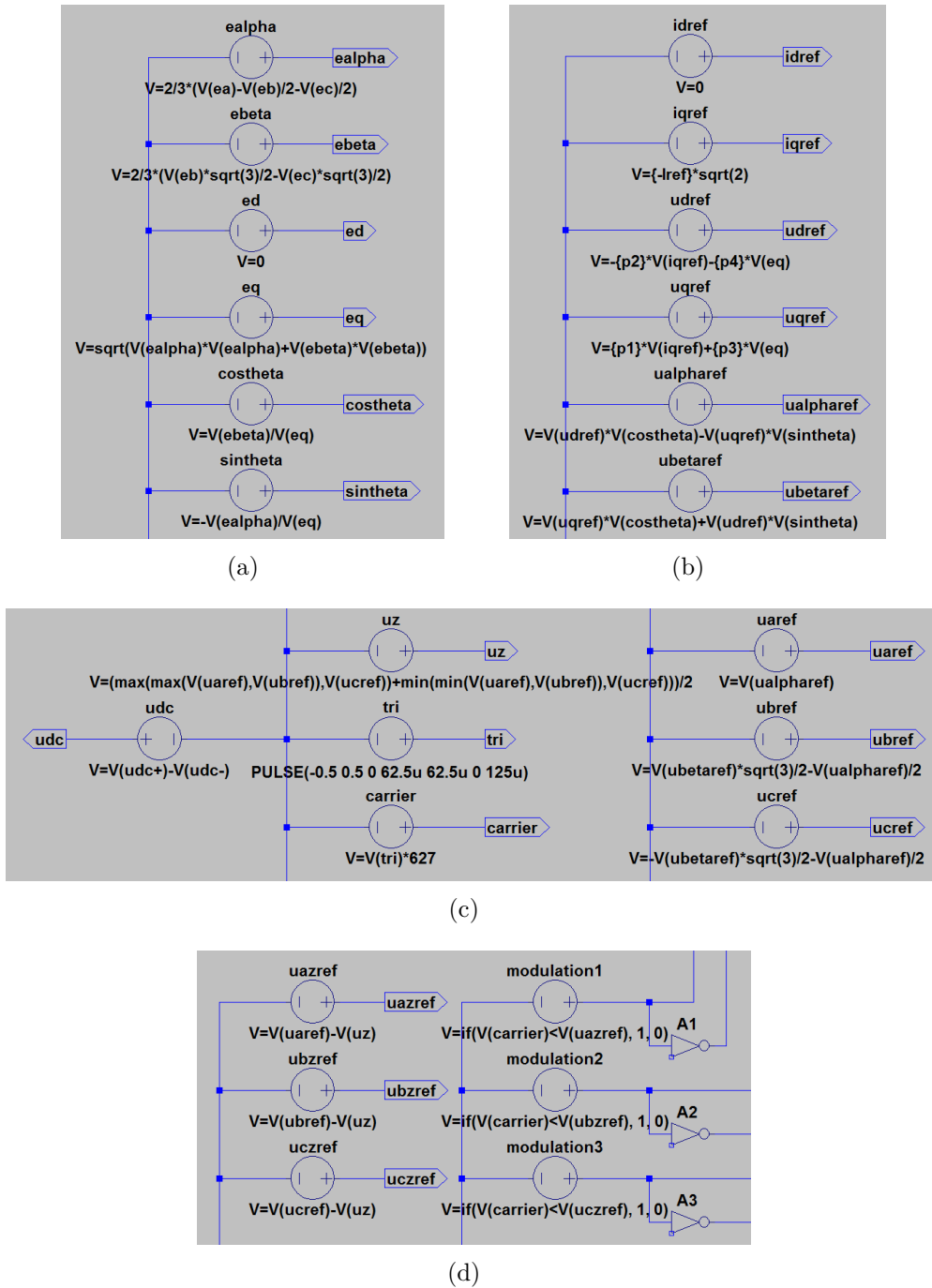
Figure 4.4: Simulation Model of the EMD Controller (LCL-Filter)

It can be observed in Figure 4.4 that the controller in the system with the LCL-filter consists of several parts. Every voltage source represents the calculation of one variable in LTspice model. Figure 4.4(a) shows how to transform three-phase stationary grid voltages to rotating dq-frame grid voltages through Park's Transformation. The rotating dq-frame grid voltage vector is fixed on the q-frame (positive) to decide the dq-frame coordinate. The rotating dq-frame line current vector will be placed on the q-frame (negative) to realize the charging function as presented in Figure 4.4(b). Hence, the value of the grid voltage and the line current reference in the rotating dq-frame is found to be

$$
\begin{aligned}
& i_{2d,ref} = 0 \\
& i_{2q,ref} = -64 \times \sqrt{2} = -90.51 \\
& e_d = 0 \\
& e_q = 400 \times \sqrt{2} \div \sqrt{3} = 326.60
\end{aligned}
\tag{4.3}
$$

It can also be observed in Figure 4.4(b) that the output voltage reference of the EMD $u_{1,ref}$ is calculated as

$$
\begin{aligned}
& u_{1d,ref} = -p_2 i_{2q,ref} - p_4 e_q \\
& u_{1q,ref} = p_1 i_{2q,ref} + p_3 e_q
\end{aligned}
\tag{4.4}
$$

in which p_1, p_2, p_3 and p_4 are calculated based on (2.32) as ($R_1 = 40\text{m}\Omega, R_2 = 20\text{m}\Omega$)

$$
\begin{aligned}
& p_1 = R_1 + R_2 - \omega_1^2(L_1 R_2 + L_2 R_1) \approx 0.0599 \\
& p_2 = \omega_1[L_1 + L_2 + C(R_1 R_2 - \omega_1^2 L_1 L_2)] \approx 0.1884 \\
& p_3 = 1 - \omega_1^2 C L_1 \approx 0.9980 \\
& p_4 = \omega_1 C R_1 \approx 0.0006
\end{aligned}
\tag{4.5}
$$

Figure 4.4(b) and 4.4(c) also show the transformation of rotating dq-frame voltage references ($u_{1d,ref}$ and $u_{1q,ref}$) to three-phase stationary voltage references ($u_{1a,ref}$, $u_{1b,ref}$ and $u_{1c,ref}$), along with the calculation of the zero-sequence signal u_z and the triangular signal u_{tri}. Figure 4.4(d) presents the symmetrical voltage modulation and six output signals are used to control the switches in the EMD. The relation of voltage vectors and current vectors in the rotating dq-frame on the AC side of the EMD is more intuitional through the vector diagram in Figure 4.5.
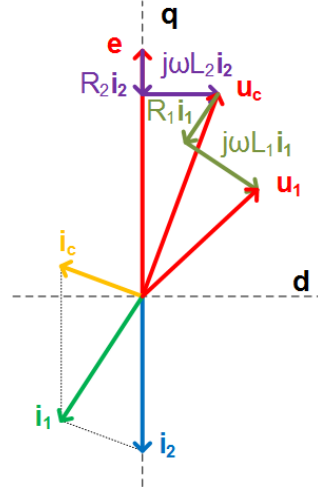
Figure 4.5: Vector Diagram (LCL-Filter)

For the L-filter, the control system has a slight change on the calculation of the voltage reference. It is mentioned before that a 8.58mH inductor will cause over-modulation, so its value should be reduced. However, the inductance still needs to be large enough to achieve a good current performance. Balancing these two conditions, some active power is sacrificed by decreasing the power factor to make the inductance as large as possible. The power factor must be higher than the lowest limit, which is 0.95[15]. Consequently, choosing the power factor angle ϕ to be 18°, the inductance can still be kept with the value of 8.58mH. The line current reference is

$$
\begin{aligned}
\cos \phi &= 0.951 \\
\sin \phi &= 0.309 \\
i_{d,ref} &= -64 \times \sqrt{2} \times \sin \phi = -27.61 \\
i_{q,ref} &= -64 \times \sqrt{2} \times \cos \phi = -86.07
\end{aligned}
\tag{4.6}
$$

Hence, the voltage reference is calculated as

$$
\begin{aligned}
u_{d,ref} &= p_1 i_{d,ref} - p_2 i_{q,ref} \\
u_{q,ref} &= p_1 i_{q,ref} + p_2 i_{d,ref} + e_q
\end{aligned}
\tag{4.7}
$$

where p_1 and p_2 calculated based on (2.33) as ($R = 50$mΩ)

$$
\begin{aligned}
p_1 &= R = 0.05 \\
p_2 &= \omega_1 L \approx 2.70
\end{aligned}
\tag{4.8}
$$

(a) Voltage Reference Calculation (b) Vector Diagram
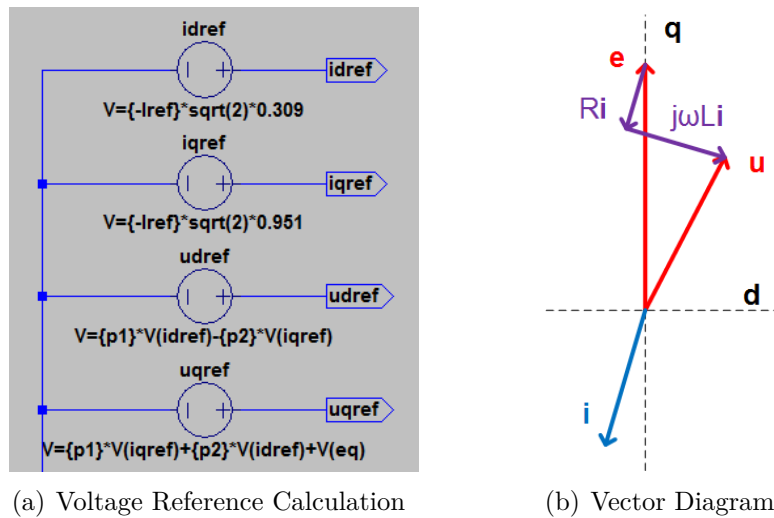
Figure 4.6: Simulation Model of the EMD Controller (L-Filter)

Figure 4.6(a) also shows how voltage references are expressed in the simulation model and a visualized vector diagram is exhibited in Figure 4.6(b) as well.

4.5 Equivalent Model

The equivalent model consists of all the remaining components in the TVS when charging the batteries through the EMD. The switch "MYSW" is to connect or disconnect the heater. The structure is exactly the same as what is shown in Figure 3.3.
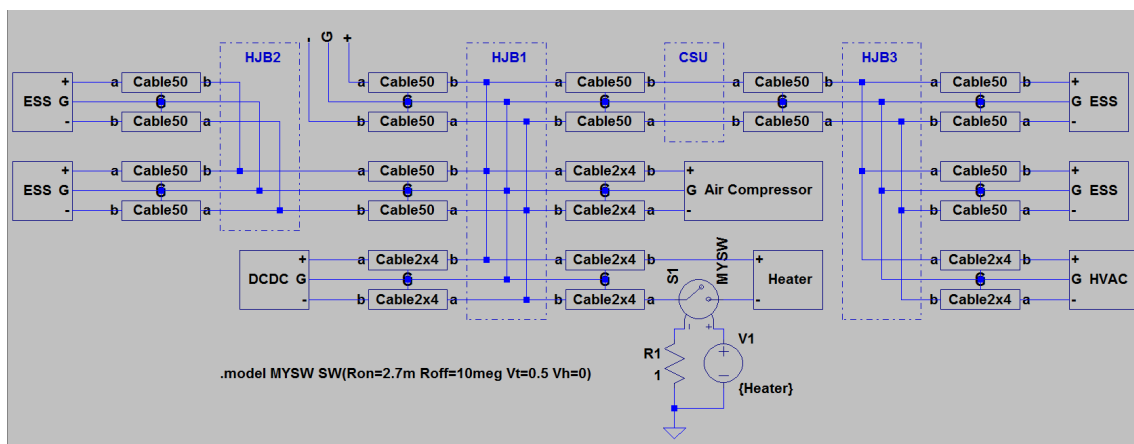
Figure 4.7: Simulation Model of the Remaining Components in the TVS

4.5.1 Energy Storage System

The ESS model is a basic battery model with one EMF, one resistor and one inductor connected in series.
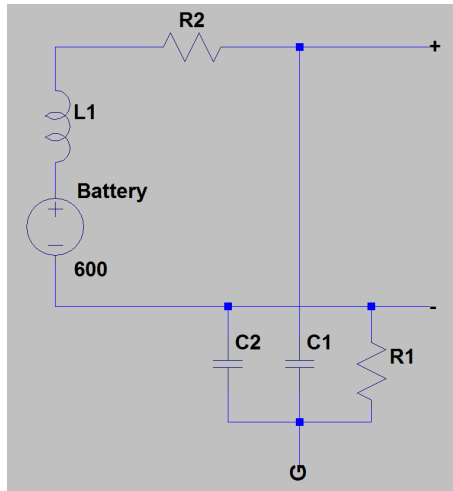
Figure 4.8: Simulation Model of the ESS

4.5.2 Heat, Ventilation and Air Condition

The HVAC model is mostly taken from data sheets and presents all the components on the DC side since they are connected to the TVS directly if the HVAC is not operating. "Ldm1" is the only component in the HVAC whose value is obtained through measurements[2].
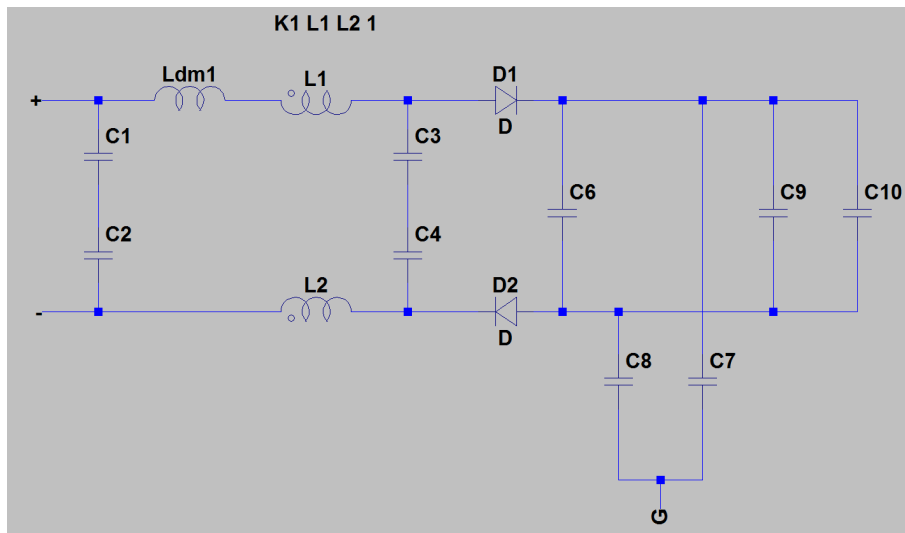
Figure 4.9: Simulation Model of the HVAC

4.5.3 Air Compressor

The Air Compressor model is similar to that of the HVAC, mostly taken from data sheets and presents all the components on the DC side. "Ldm1" is the only component in the Air Compressor whose value is obtained through measurements[2].
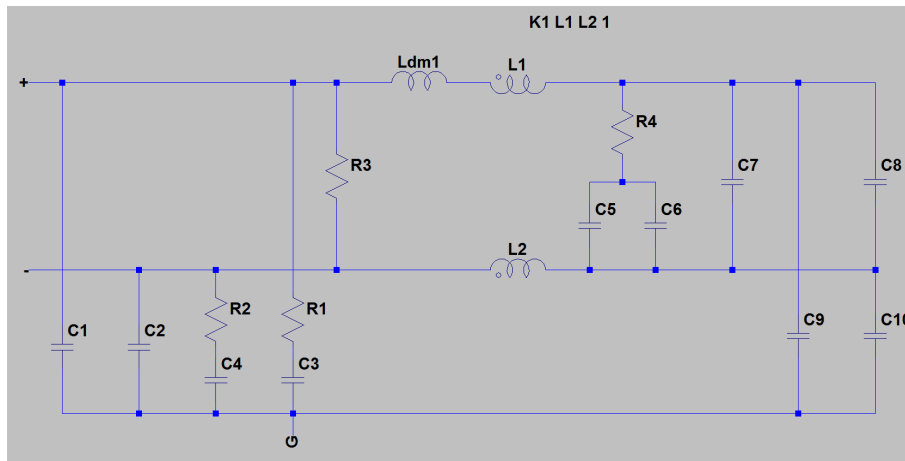
Figure 4.10: Simulation Model of the Air Compressor

4.5.4 DC/DC Converter

The DCDC model only contains components on the DC side as well. However, it might be operational during the charging period. The simplest method to simulate that condition is to parallel connect a current source after "C3" to represent the load. "L5" is the only component in the DCDC whose value is obtained through measurements[2].
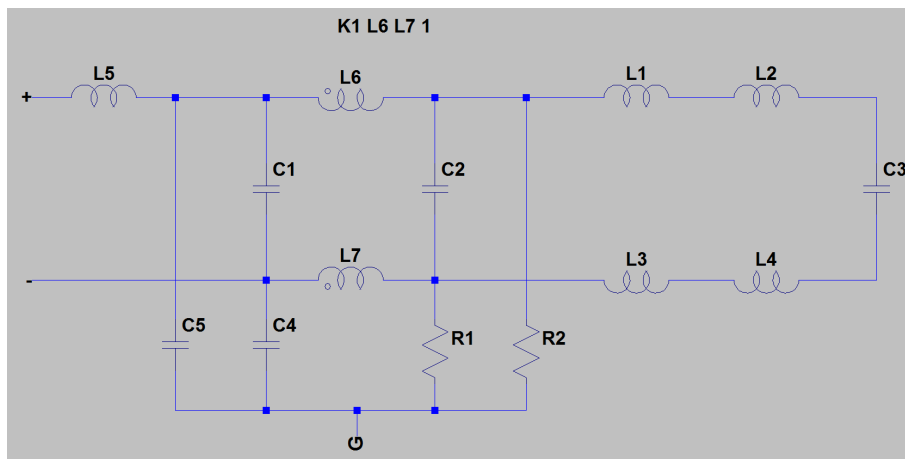
Figure 4.11: Simulation Model of the DCDC

4.5.5 Cable

The cable models are the same in terms of the structure and the only difference is values of the resistance, the inductance and the capacitance.
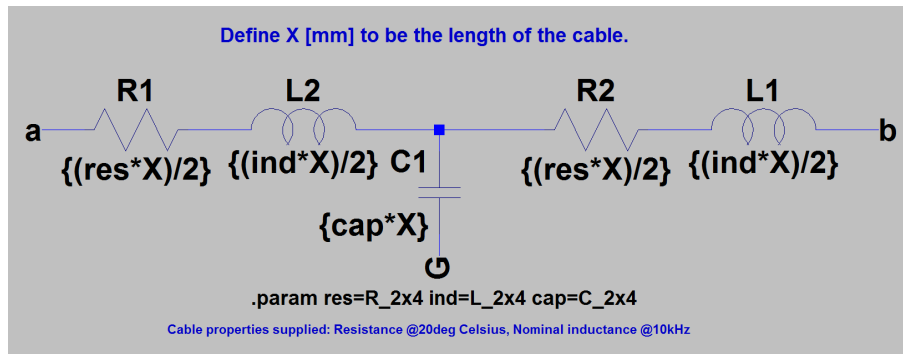
(a) $2 \times 4\text{mm}^2$
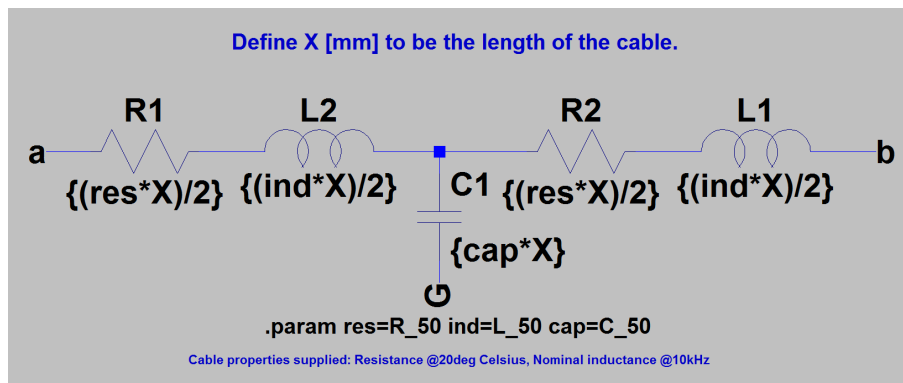
(b) 50mm^2

Figure 4.12: Simulation Model of the Cables

4.5.6 Auxiliary Heater

The heater is a pure resistive load.
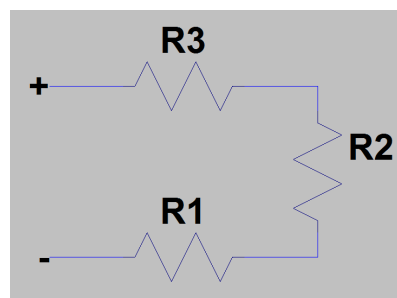
Figure 4.13: Simulation Model of the Heater

4.6 Touch Current

As described before, the touch current is a significant parameter when designing the charging system. When simulating the measurement of the touch current, how the measurement module is connected is presented in Figure 4.14(a), which is the same

set up as what is shown in Figure 3.4. Figure 4.14(b) shows the inner circuit of the measurement module.

(a)

(b)
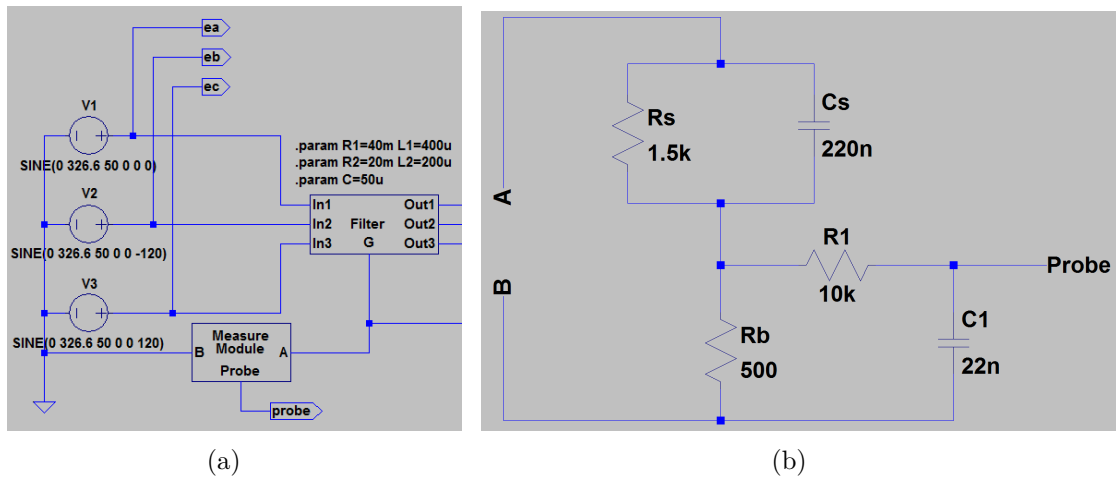
Figure 4.14: Simulation Model of Measuring the Touch Current

5

Result

The parameters of the filter designed in the previous section are aimed to realize the requirement of the Total Harmonic Distortion (THD) of the line current on the grid side[9]. It will also be investigated whether this charging system fulfills requirements of the inrush current, the touch current and the grounding current. Simulation results of the charging system with either the L-filter or the LCL-filter will be presented in following sections.

5.1 Charging Performance
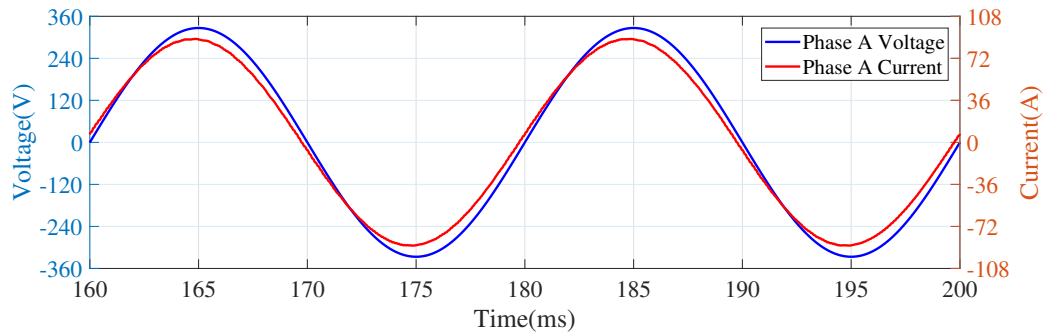
(a) Input Voltage and Current
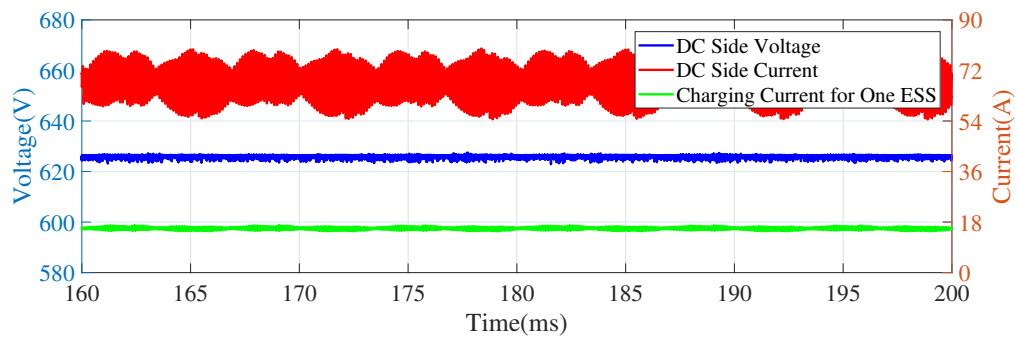
(b) Output Voltage and Current

Figure 5.1: Charging System Performance (LCL-Filter)

The charging performance is evaluated mainly through the THD and the efficiency. For each system with the different filter, the input voltage and current from the

grid, along with the output voltage and current of the EMD are extracted to plot the waveform. Meanwhile, the current flowing into the ESS is measured as well to calculate the charging efficiency. The charging performance of the system with the LCL-filter is shown in Figure 5.1. The charging efficiency η and THD of the line current is calculated as

$$
\begin{aligned}
P_{inLCL} &= \sqrt{3}U_N I_N \cos\phi \approx 43.16\text{kW} \\
P_{outLCL} &= U_d I_d \approx 41.61\text{kW} \\
\eta_{LCL} &= \frac{P_{out}}{P_{in}} \times 100\% \approx 96.41\% \\
THD_{LCL} &= \frac{\sqrt{\sum_{h=2}^{\infty} I_h}}{I_1} \times 100\% = \frac{\sqrt{I^2 - I_1^2}}{I_1} \times 100\% \approx 0.57\%
\end{aligned}
\tag{5.1}
$$

where I_h, I_1 and I represent the RMS value of the hth order harmonic in the line current, the fundamental component in the line current and the total line current.
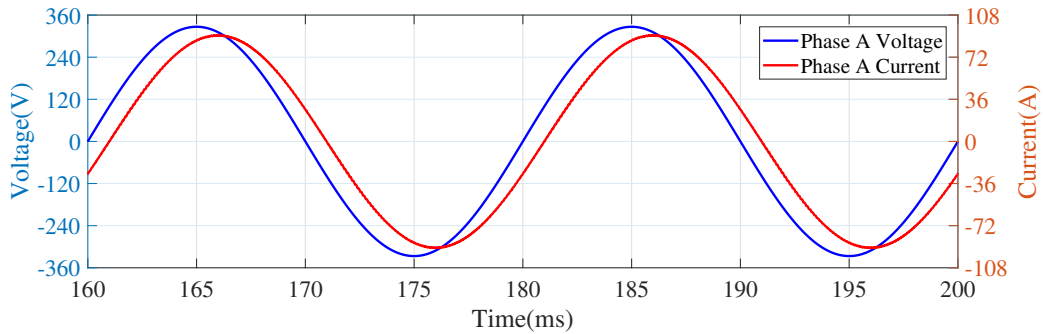
(a) Input Voltage and Current
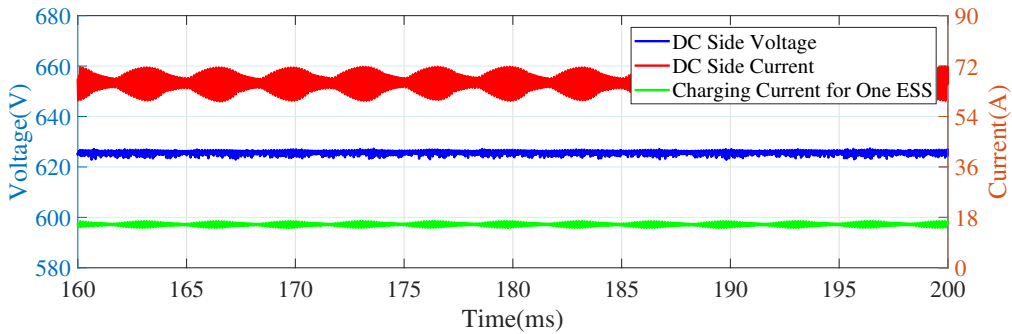
(b) Output Voltage and Current

Figure 5.2: Charging System Performance (L-Filter)

The charging performance of the system with the L-filter is shown in Figure 5.2.

The charging efficiency η and THD of the line current is calculated as

$$P_{inL} = \sqrt{3} U_N I_N \cos\phi \approx 42.35\text{kW}$$
$$P_{outL} = U_d I_d \approx 40.92\text{kW}$$
$$\eta_L = \frac{P_{out}}{P_{in}} \times 100\% \approx 96.62\%$$
$$THD_L = \frac{\sqrt{\sum\limits_{h=2}^{\infty} I_h}}{I_1} \times 100\% = \frac{\sqrt{I^2 - I_1^2}}{I_1} \times 100\% \approx 0.27\%$$

(5.2)

It is obvious that the LCL-filter achieves a similar charging performance in terms of THD with much smaller inductances compared to that in the case of an L-filter, which means the LCL-filter requires less space and lower cost than the L-filter. The efficiency is just to provide a concept since the resistance of most components are just set to be a small value without measurements, like 10mΩ. In reality, some components in the TVS, for instance, the DCDC would be operational. They will also consume more power and reduce the efficiency.

5.2 Inrush Current

The inrush current occurs at the point of supply the system with the highest supply voltage and shall not exceed 230A within 100μs limited by the regulation[15]. For the L-filter, there will be no current even though the power supply is connected, until the EMD starts to operate. However, there will be current flowing through outer inductors and capacitors in the LCL-filter to the ground as long as the power supply is connected. Consequently, only the LCL-filter has an inrush current needed to be simulated after closing the contactor in the EV supply equipment at the peak value of the supply.

Since initial conditions of the output voltage of the EMD are already defined in the LTspice model (see Appendix A), its starting conditions cannot be the same as what is fined in the regulation[15]. Simulating the starting process will be conducted in Simulink based on the transfer function of the LCL-filter. The equivalent circuit is one outer inductor and a capacitor connected in series, so the transfer function is derived as

$$G(s) = \frac{I(s)}{U(s)} = \frac{1}{R_2 + L_2 s + \frac{1}{Cs}}$$
$$= \frac{Cs}{L_2 C s^2 + R_2 C s + 1} = \frac{5 \times 10^{-5} s}{1 \times 10^{-8} s^2 + 1 \times 10^{-6} s + 1}$$

(5.3)

Applying the highest phase voltage of 326.6V in the step voltage source, the inrush current will reach 136.7A at 100μs as presented in Figure 5.3.
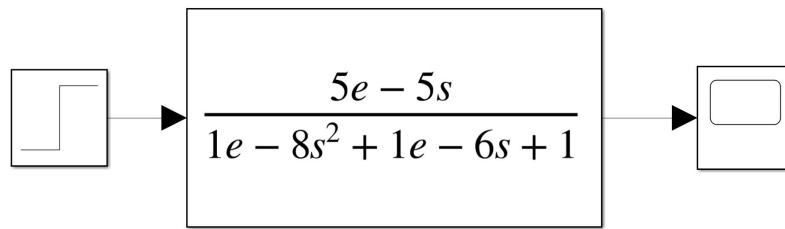
(a) Simulink Model
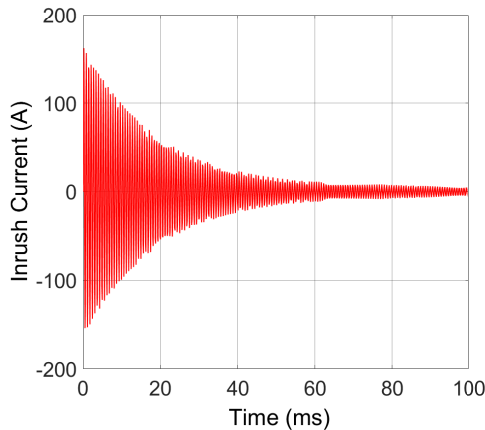
(b) Inrush Current
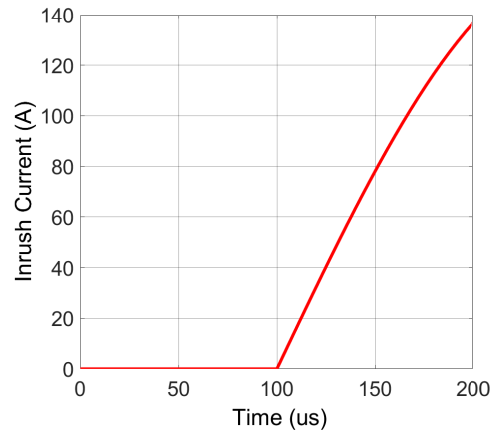
(c) Inrush Current in $100\mu s$

Figure 5.3: Inrush Current Simulation (LCL-Filter)

5.3 Grounding Current and Touch Current

The grounding current, also known as leakage current, is measured in the grounding resistor and it should be within the limit of 30mA[14]. Replacing the grounding resistor with the measurement module exhibited in Figure 4.14(b), the touch current is obtained and should be smaller than 3.5mA[15].

It is founded that only the system with the LCL-filter meets the requirements for these two indexes and Figure 5.4 shows simulation results of the grounding current and the touch current between 160ms and 200ms. It can be observed from the simulation that the grounding current can reach the steady state in 200ms, while the touch current cannot due to the time constant of the measurement module. Hence, a longer simulating time is applied and the system turns out to have a grounding current of 2.47mA and a touch current of 0.22mA. In addition, enlarging the grounding resistance will reduce the grounding current, but it needs to be further investigated whether it is feasible in the real application.

(a) Grounding Current
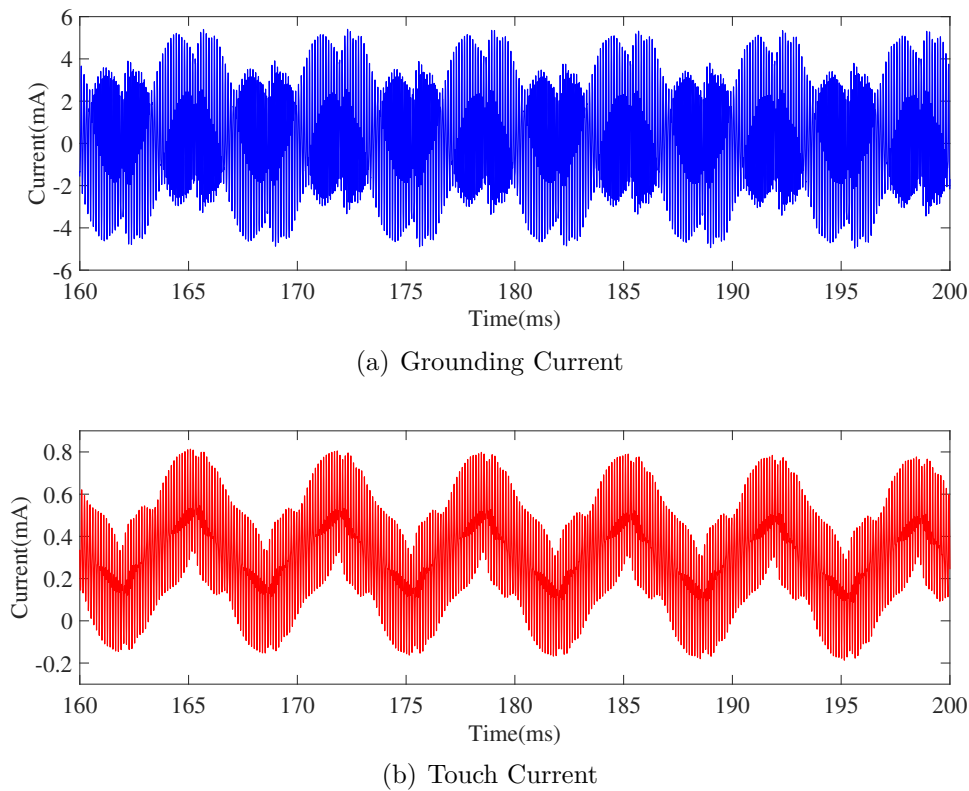
(b) Touch Current

Figure 5.4: Grounding Current and Touch Current (LCL-Filter)

5.4 Dimension, Weight and Cost

The additional cost comes from the added devices, which are one filter and one CMSB. The components needed in these two devices are listed in Table 5.1

Table 5.1: Specification Values of Required Components in the LCL-Filter and the Switch Box

Component	Value	Rated Voltage (V)	Rated Current (A)
Inductor L_1	$400\mu H$	$\geqslant 230$	$\geqslant 64$
Inductor L_2	$200\mu H$	$\geqslant 230$	$\geqslant 64$
Capacitor C	$50\mu F$	$\geqslant 230$	$\geqslant 3.2$
Contactor	-	$\geqslant 400$	$\geqslant 64$

It can be seen that the inductors and the capacitors should be able to withstand the rated phase voltage. The inductors require a rated current which is the same as the rated line current, while the capacitors are designed to withstand 5% of the nominal line current as described in the theory. Since the contactor is a three-phase device, the voltage and current requirement for it is the rated line voltage and the nominal line current.

39
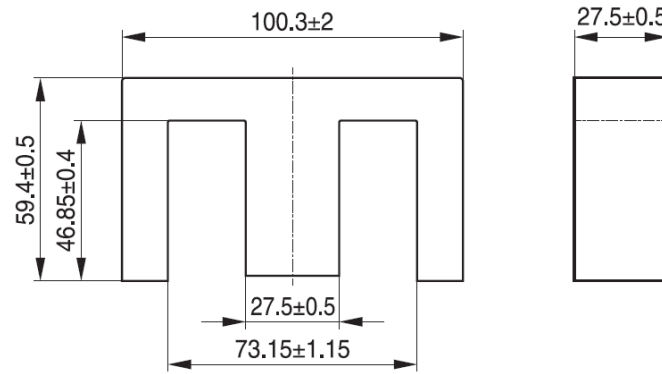
Figure 5.5: Ferrite Core Dimension

Applying (2.34)~(2.37), the inductor can be designed. A ferrite core is selected. Its material is N95 and its dimensions are presented in Figure 5.5. The effective length l_e of one set is 274mm and the effective area A_e is 735mm^2. The relative permeability of the ferrite core is 2520. A 4mm air gap is designed for this inductor, so the equivalent relative permeability of the inductor is calculated with (2.36)

$$\mu_r = \frac{\mu}{\mu_0} = \frac{\mu_c(l_c + l_g)}{\mu_0 l_c + \mu_c l_g} = 67 \tag{5.4}$$

. Hence, with (2.37), the inductor L_2 is designed as

$$
\begin{aligned}
R &= \frac{l_c + l_g}{\mu A_c} \approx 4.33 \times 10^6 \\
N_2 &= \sqrt{L_2 R} \approx 30 \\
B_2 &= \frac{\Phi}{A_c} = \frac{NI}{A_c R} \approx 0.60\text{T}
\end{aligned}
\tag{5.5}
$$
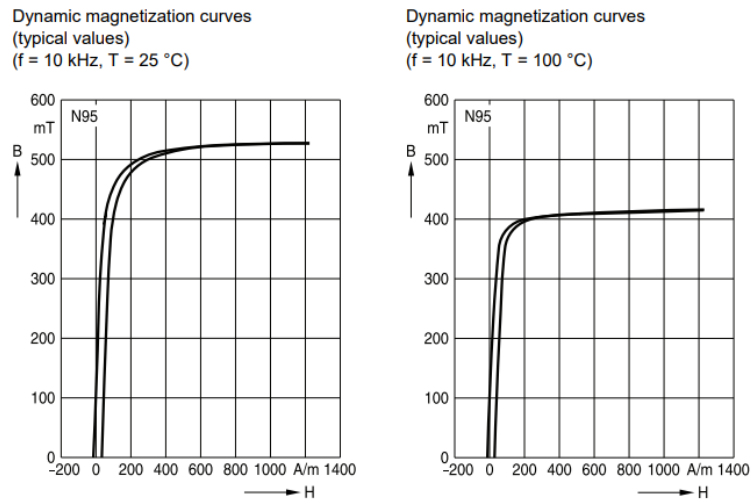
Figure 5.6: Ferrite Core Hysteresis Curve

What is shown in Figure 5.6 is the hysteresis curve of the N95 material. The flux density in the core should be kept within the linear range of this curve. Hence, a flux density of 0.2T is chosen. Apparently, the flux density calculated previously is too large. Consequently, the filter design is recalculated using combined ferrite cores to increase the volume of the core and reduce the flux density. Nine cores are utilized to obtain the ferrite core in L_2.

$$R = \frac{l_c + l_g}{9\mu A_c} \approx 4.81 \times 10^5$$
$$N_2 = \sqrt{L_2 R} \approx 10 \tag{5.6}$$
$$B_2 = \frac{\Phi}{9A_c} = \frac{N_2 I}{9A_c R} \approx 0.20\text{T}$$

The total length of wires used in the winding is at least $2 \times (27.5 + 9 \times 27.5) \times 10 = 5500$mm. The conducted area of the wire is 16mm^2 with a rated current of 76A and the density of copper is 8.96g/cm^3. So, the weight of the conductor is 0.79kg. Since the mass of the core is 987g, the weight of this inductor m_2 is approximately 9.67kg. Eighteen ferrite cores are used in L_1 and parameters of L_1 are calculated to be $N_1 = 10, B_1 = 0.20$T and $m_1 = 18.56$kg. The cost of single ferrite core unit is about 157SEK, and the price of copper is around 64SEK/kg. Hence, the manufacture cost of L_1 is at least 5703SEK and the cost of L_2 is at least 2877SEK.
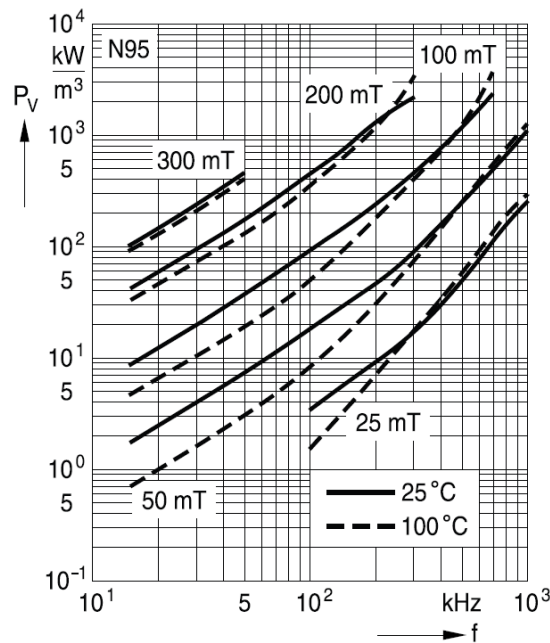
Figure 5.7: Ferrite Core Relative Core Losses

It is also important to calculate the losses in the inductor. Losses in the inductor is the sum of core losses and resistive losses. Figure 5.7 shows the relative core losses in the core material N95. Since the switching frequency in this case is 8kHz, the value of relative core losses at 0.2T is found to be 300kW/m^3. The effective volume

of one core set is 201390mm^3. Since nine core sets are utilized in L_2, the core losses in it is equal to 543.75W. The resistivity of the copper is $1.75 \times 10^{-8}\Omega$m, so the resistor of the copper wire in L_2 is 6.02mΩ. The resistive losses in the copper wire is calculated as the active power that it consumes, which is 24.64W. Hence, the total losses in L_2 is 568.39W. Similarly, the total losses in L_1 is calculated to be 1134.32W. Consequently, the total losses of inductors in the filter would be 5.11kW. Using different core materials in the filter and optimizing the structure of the core could help to decrease the losses.

The calculations above provide an idea of some influences the filter could bring to the system. However, the isolation, connections and other aspects are not considered yet, which implies that the actual weight might be larger than the calculation. Since it is a rough calculation, the information from the manufacturer is also presented. What is shown in Table 5.2 is a rough estimate about dimensions, weights and costs of the required additional components in this system after searching for similar products on the website. The casings of devices containing these components are not considered.

Table 5.2: Dimension, Weight and Cost of Required Components in the LCL-Filter and the Switch Box

Component	Dimension (mm)	Weight (kg)	Cost (SEK)
Inductor L_1	$134 \times 140 \times 114$	11.8	3230
Inductor L_2	$191 \times 178 \times 166$	20.9	3753
Capacitor C	$65 \times 65 \times 138$	0.4	314
Contactor	$147 \times 106 \times 79$	-	1748

This information provides an approximate concept about dimensions and costs of the added devices. Considering connections, layouts and casings of those components, the size of the filter and the CMSB is approximately 50L and they have a weight of more than 100kg. The total cost of them is about thirty thousand SEK. The OnBC in the previous system has a volume of 15L, a weight of 15kg and a cost of twenty thousand SEK. It can be seen that this solution does not have advantages in terms of these aspects. However, four OnBCs are needed if the charging power needs to reach 44kW. Considering this term, the filter is cheaper and smaller than four OnBCs, but only with larger mass.

5.4.1 Parameter Analysis

According to the inductor design, it is found that a filter with smaller inductance will create more benefits. Consequently, three parameters that could affect the inductor design will be discussed to provide ideas about limiting the size of the filter.
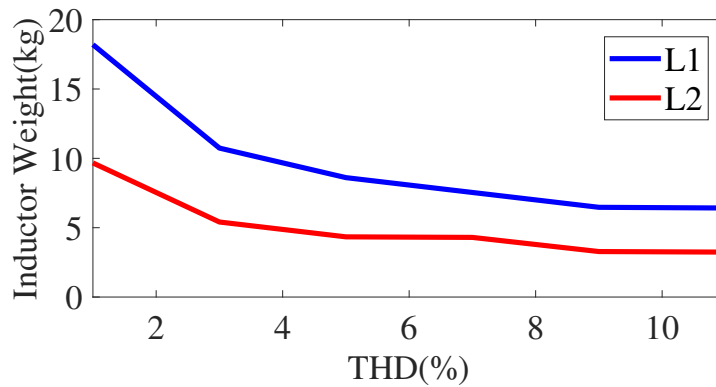
Figure 5.8: Inductor Weight - THD of Line Current

Figure 5.8 shows that the weight of inductors needed for the LCL-filter will decrease when the tolerance of THD of the line current is higher. However, a higher THD will also lead to a larger grounding current. So, the safety margin of the grounding current needs to be maintained when adjusting the requirement of THD.
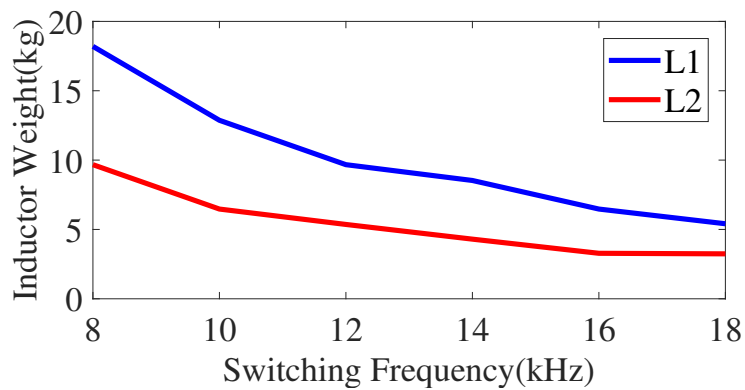
Figure 5.9: Inductor Weight - Switching Frequency

Figure 5.9 presents the weight of inductors when choosing different switching frequencies of the EMD. The harmonic component at the switching frequency of the EMD is the largest harmonic component in the line current. Increasing switching frequency could help to reduce the size of inductors in the filter. The advantage of using higher switching frequency to limit the size of the filter is that it will not affect THD of the line current. Hence, the grounding current can still be kept at a low value. However, more switching losses could also be a problem when utilizing higher switching frequency.
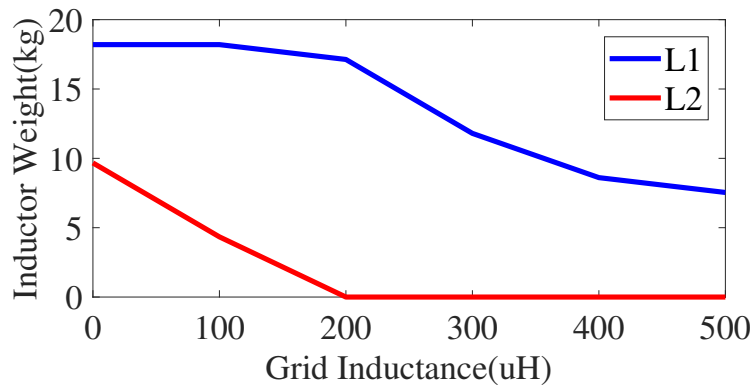
Figure 5.10: Inductor Weight - Grid Inductance

The grid inductance was assumed to be zero in the simulation, since the power grid is viewed as a strong grid. In reality, the grid inductance will have different values at different charging stations. When the grid inductance is larger than 200μH, the LCL-filter can even be simplified into an LC-filter. A possible method to limit the size of the filter by the grid inductance is provided as well. First, the value of the grid inductance can be divided into several levels. Second, a filter will be designed for each level based on the worst case in that level. After that, measurements will be conducted for different charging stations to identify the accurate value of the grid inductance. At last, a suitable filter design is selected based on the measurement result.

5.5 Discussion

In the solution provided, several aspects require attention:
- An inductor which has a value of hundreds μH and can withstand more than 64A is definitely large and heavy according to the information obtained on the Internet. Hence, the solution explored in this thesis will not have advantages in terms of dimensions, weights and costs, which means that they will not be the main focus when adjusting parameters in the filter.
- The touch current will be small because of the large resistance of the measurement module. However, there might be some problems with the grounding current. The grounding current of 2.47mA is achieved with a grounding resistance of 500Ω. This grounding resistance might not be realized in practical applications, because the tools connecting the power supply and the vehicle during charging are just cables, and the resistance of them is close to zero. If it is impossible to implement a resistor between the chassis and the power supply, the grounding current will be far beyond the limit.
- It is noticed that increasing the capacitance in the filter will reduce the grounding current, since the higher capacitance makes high frequency harmonics pass through more easily. However, the higher capacitance will also increase the current in capacitors and inner inductors. Consequently, the capacitance can increase in a reasonable range when considering the rated current of cables connecting the EMD.

- The symmetrical modulation used in the controller of the EMD will introduce the 3rd order harmonic into the the grounding current, which increases its value. Applying sinusoidal modulation can prevent it, but it is necessary to be careful with over-modulation. Either decreasing the power factor or increasing the battery voltage could help to prevent that.
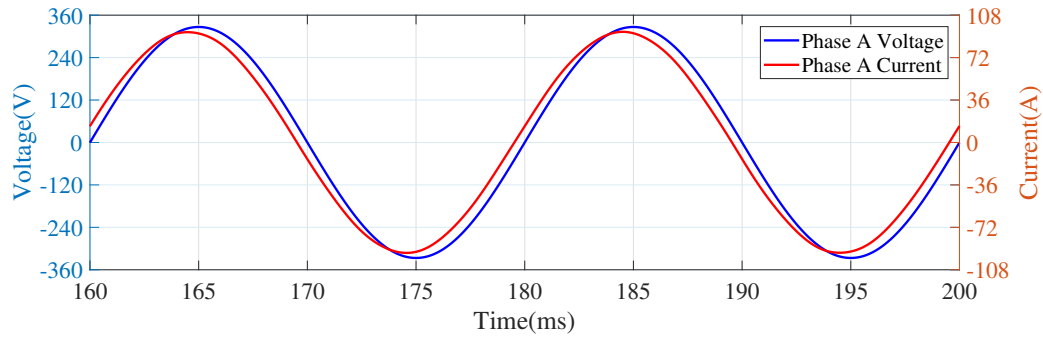
(a) Input Voltage and Current
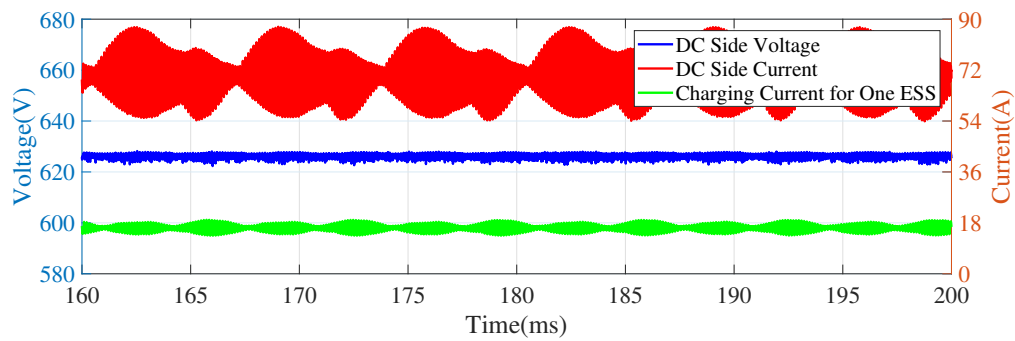
(b) Output Voltage and Current
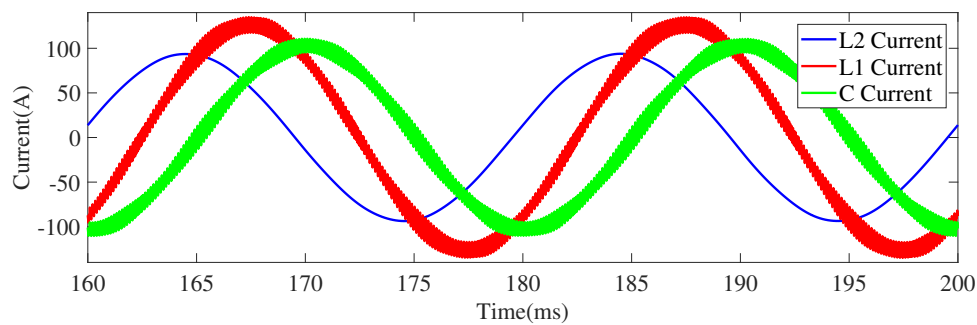
(c) Filter Current

Figure 5.11: Charging System Performance (LCL-Filter with Larger Capacitance)

Based on these problems, another solution is provided. The modulation scheme is going to be sinusoidal modulation. The grounding resistance is set to be 0.1mΩ. The parameters in the filter are chosen to be $L_1 = 500\mu$H, $L_2 = 250\mu$H and $C = 1$mF. The charging performance is shown in Figure 5.11. The charging efficiency η and

THD of the line current is calculated as

$$P_{inLCL} = \sqrt{3}U_N I_N \cos\phi \approx 45.41\text{kW}$$
$$P_{outLCL} = U_d I_d \approx 43.18\text{kW}$$
$$\eta_{LCL} = \frac{P_{out}}{P_{in}} \times 100\% \approx 95.08\% \tag{5.7}$$
$$THD_{LCL} = \frac{\sqrt{\sum\limits_{h=2}^{\infty} I_h}}{I_1} \times 100\% = \frac{\sqrt{I^2 - I_1^2}}{I_1} \times 100\% \approx 0.55\%$$

The slight reduction in the efficiency results from that the series resistance in inner inductors will consume more active power with a higher current. The current in the capacitor C is 72.65A and the current in the inner inductor L_1 is 89.54A. The inrush current of this filter is 129.3A at the point of $100\mu s$ as shown in Figure 5.12.

(a) Simulink Model

(b) Inrush Current

(c) Inrush Current in $100\mu s$
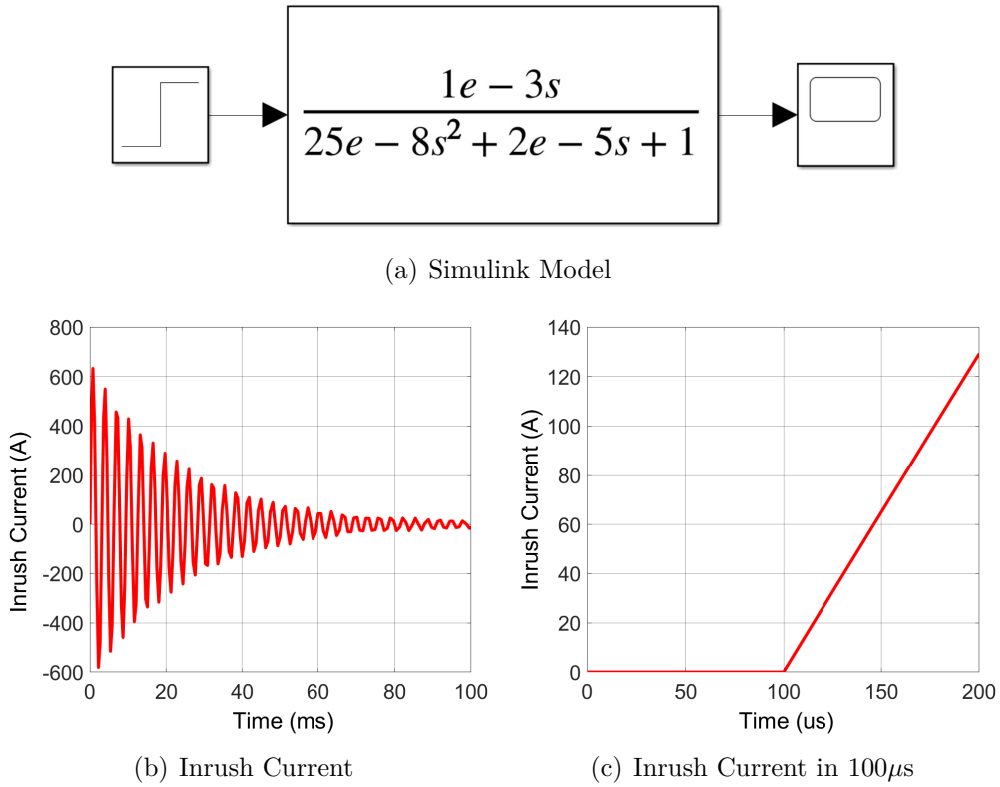
Figure 5.12: Inrush Current Simulation (LCL-Filter with Larger Capacitance)

Figure 5.13 presents simulation results of the grounding current and the touch current between 160ms and 200ms. The same problem occurs that it takes a longer time for the touch current to reach the steady state. Applying with a sufficiently long simulating time, the result shows that the grounding current is about 14.94mA and the touch current is approximately 0.01mA.

(a) Grounding Current
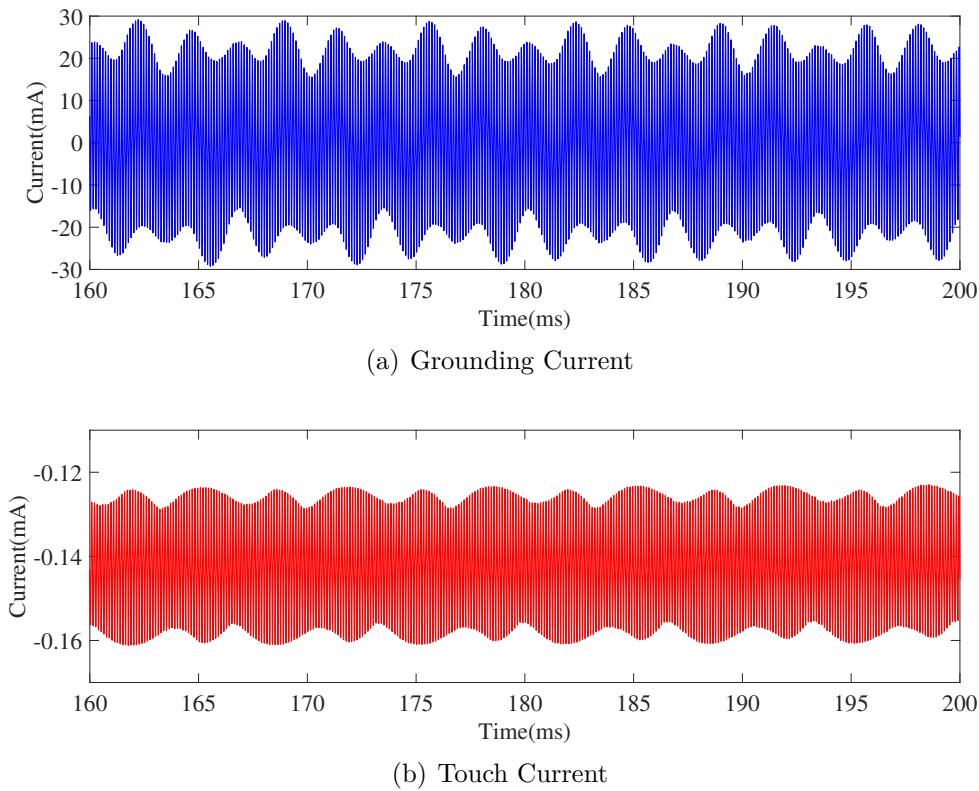
(b) Touch Current

Figure 5.13: Grounding Current and Touch Current (LCL-Filter with Larger Capacitance)

After sourcing for similar products on the Internet, dimensions, weights and costs of the required components in the filter is exhibited in Table 5.3.

Table 5.3: Dimension, Weight and Cost of Required Components in the LCL-Filter (Larger Capacitance)

Component	Dimension (mm)	Weight (kg)	Cost (SEK)
Inductor L_1	$134 \times 140 \times 114$	11.8	3230
Inductor L_2	$191 \times 178 \times 166$	20.9	3753
Capacitor C	$116 \times 116 \times 150$	1.7	1271

Considering connections, layouts and casings of those components, the size of the filter and the CMSB is approximately 60L and they have a weight of about 150kg. The total cost of them is about thirty-five thousand SEK. If the cables and all the components can withstand higher current, the capacitance in the filter can be increased more, which ensures a larger margin for the grounding current.

6
Conclusion

This thesis is aimed to redesign and simulate the charging system to increase the charging power, which is also the main purpose of conducting the project. Since the EMD is designed for a harsher environment, the robustness of the system could be increased. Besides, Volvo does not own the design of the OnBC. Utilizing the EMD also as an AC-charger provides higher flexibility of adjustments inside the TVS.

From the result chapter, it can be concluded that the LCL-filter does have a better performance than the L-filter. The LCL-filter is able to meet all the requirements and it is a feasible solution to this project from the view of simulation. Moreover, when using these two charging solutions to achieve the same charging power, the design of the integrated non-isolated AC-charger requires less space and cost than the four OnBCs required. However, the added devices, which are the filter and the CMSB, are heavier than four OnBCs. The values of promoting this solution in the practical application needs more investigations.

From the calculation of the losses of the inductors in the filter, the value is a bit high considering the charging power. This might be solved with different core materials and core structures. To limit the size of the filter, it is suggested to increase the switching frequency. To limit the grounding current, a larger capacitance in the LCL-filter and applying sinusoidal modulation would be a better option. However, that could result in a strong current in the capacitor and over-modulation problem, which should be avoided by adjusting parameters carefully.

6.1 Future Work

This project proves that the solution is feasible from the simulation perspective. The future work could include several aspects:
- The power grid model needs to be optimized based on actual conditions in different charging stations. The model of each device can be improved as well.
- Redesign of the internal circuit of the EMD is also possible. If transformer design can be implemented inside the EMD, the grounding current and the touch current will be easier to limit.
- The investigation about whether extra cooling system is needed for the added switch box and filter is necessary.
- The programming in the EMD to realize the function is required. The testing on a prototype bus to see whether it could achieve all the requirements in the

practical application is also necessary to evaluate the result of simulations.

- How much capacitance is acceptable needs to be explored, which depends on the rated current of components in the filter and cables connected to it.
- Simulating different core materials and structures to limit the weight and losses of the inductors.
- One disadvantage of utilizing the EMD as an AC-charger is that the EMD will be operational all the time, which will shorten its life time. How much influence this solution will generate on the life time of the EMD needs to be investigated as well.
- Whether it is worthy of implementing such huge filter and switch box on the vehicle also needs to be identified.

Bibliography

[1] C. Lugnberg and D. Wenander, "Current Ripple Simulation in DC Traction Voltage System of an Electric Bus", Master Thesis, Department of Industrial Electrical Engineering and Automation (IEA), Lund Institute of Technology, Lund, Sweden, January 2017.

[2] F. Gard and L. Nilsson, "Current Ripple Simulation in DC Traction Voltage System of an Electric Bus: 2", Master Thesis, Department of Industrial Electrical Engineering and Automation (IEA), Lund Institute of Technology, Lund, Sweden, June 2017.

[3] European Commision, "Communication from the Commission to the European Parliament, the Council, the European Economic and Social Committee and the Committee of the Regions: A Policy Framework for Climate and Energy in the Period from 2020 to 2030", https://eur-lex.europa.eu/legal-content/EN/TXT/?uri=CELEX:52014DC0015, January 2014.

[4] S. Yedla, *Urban Transportation and the Environment: Issues, Alternatives and Policy Analysis.* Springer India, 2015.

[5] N. Mohan, T. M. Undeland, and W. P. Robbins, *Power Electronics: Converters, Applications and Design*, 3rd ed. John Wiley & Sons, 2007.

[6] P. Karlsson, "Quasi Resonant DC Link Converters - Analysis and Design for a Battery Charger Application", Licentiate Thesis, Department of Industrial Electrical Engineering and Automation (IEA), Lund Institute of Technology, Lund, Sweden, November 1999.

[7] M. Alakula and P. Karlsson, "Power Electronics: Devices, Converters, Control and Applications", Department of Industrial Electrical Engineering and Automation (IEA), Lund Institute of Technology, Lund, Sweden, 2015.

[8] Y.-S. Lai and S. R. Bowes, "Optimal Bus-Clamped PWM Techniques for Three-phase Motor Drives", *The 30th Annual Conference of the IEEE Industrial Electronics Society*, vol. 2, pp. 1475–1480, November 2004.

[9] United Nations, "Agreement Concerning the Adoption of Uniform Technical Prescriptions for Wheeled Vehicles, Equipment and Parts which can be Fitted and/or be Used on Wheeled Vehicles and the Conditions for Reciprocal Recognition of Approvals Granted on the Basis of these Prescriptions, Addendum 9: Regulation No. 10", October 2014.

[10] M. Lindgren, "Filtering and Control of a Grid - Connected Voltage Source Converter", Licentiate Thesis, Department of Electric Power Engineering, Chalmers University of Technology, Gothenburg, Sweden, September 1995.

[11] M. Bojrup, "Advanced Control of Active Filters in a Battery Charger Application", Licentiate Thesis, Department of Industrial Electrical Engineering and

Automation (IEA), Lund Institute of Technology, Lund, Sweden, December 1999.

[12] R. H. Park, "Two-Reaction Theory of Synchronous Machines Generalized Method of Analysis - Part I", *Transactions of the American Institute of Electrical Engineers*, vol. 48, pp. 716–727, July 1929.

[13] P. C. Krause, O. Wasynczuk, and S. D. Sudhoff, *Analysis of Electric Machinery and Drive Systems*, 2nd ed. Wiley Interscience, John Wiley & Sons. INC., 2013.

[14] International Electrotechnical Commission (IEC), "International Standard IEC61851-1 Electric Vehicle Conductive Charging System - Part 1: General Requirements", February 2017.

[15] Swedish Standards Institute, "Svensk Standard SS-EN ISO 17409:2017 Electrically Propelled Road Vehicles - Connection to an External Electric Power Supply - Safety Requirements", January 2017.

A

LTspice Instruction

LTspice is a strong electrical simulation tool applied in this thesis. Consumers can select any component in the component option shown in Figure A.1 or define their own components and devices.
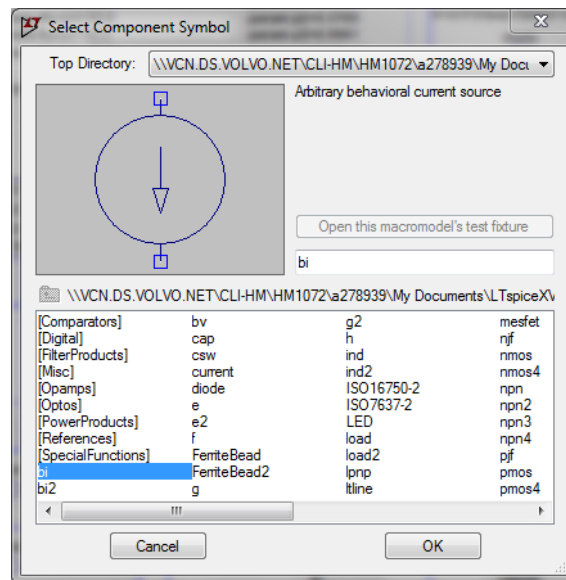
Figure A.1: Component Option

A circuit or a system is formed by connection between different components and devices. After making sure that no point is floating, the simulation can be run. Since all the components are models of real objects, there is not any component can do calculation like matrix multiplication, which is one shortage compared to Simulink. One independent voltage source should be created for each variable as presented in Figure 4.4.

In addition when the system becomes too complex, it is necessary to decrease the accuracy of the simulation to increase its speed. This can be achieved by adding "SPICE Directive" instead of making adjustments in the "Control Panel" every time, which is defined as ".options Gmin=1E-6 Abstol=1E-6 Reltol=1E-3 Chgtol=1E-6". "Gmin=1E-6" means adding a small conductance of 1e-6 ($= 1\text{M}\Omega$) parallel to every diode of transistors and diodes. "Abstol=1E-6" implies that increasing the allowed tolerance from 1e-12 to 1e-6 for the convergence criteria. "Reltol=1E-3" shows that the allowed tolerance is 0.001 for the convergence criteria and it is not allowed to

be larger than 0.003. "Chgtol=1E-6" means capacitance added from each node to ground is $1\mu F$. Adding a small CSHUNT to each node can solve some "internal timestep too small" problems caused by high-frequency oscillations or numerical noise.

In this thesis, the resistance of each inductor is small, which would cause extremely large current at the beginning of simulation. As a result, it will take longer time to reach steady state and sometimes the simulation cannot continue. To prevent this from happening, "SPICE Directive" is also necessary.
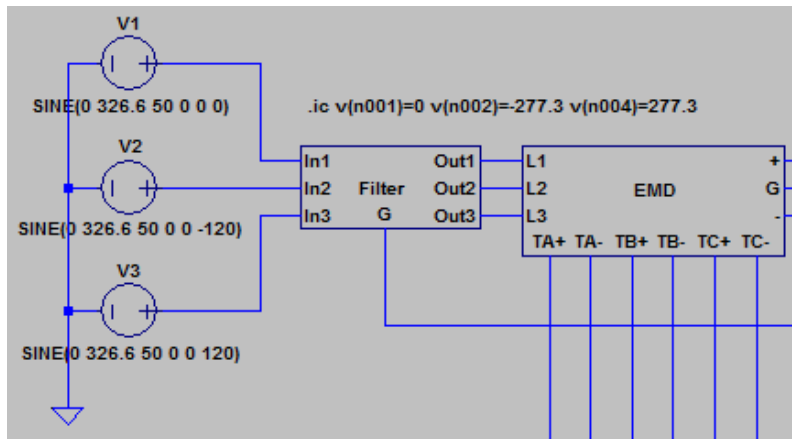
Figure A.2: Initial Condition

As can be observed in Figure A.2, ".ic v(n001)=0 v(n002)=-277.3 v(n004)=277.3" set the default value of the voltage at "L1 L2 L3" points of the EMD. By doing so, the voltage difference over the filter is very close to the value at steady state, which makes the simulation operate more smoothly.
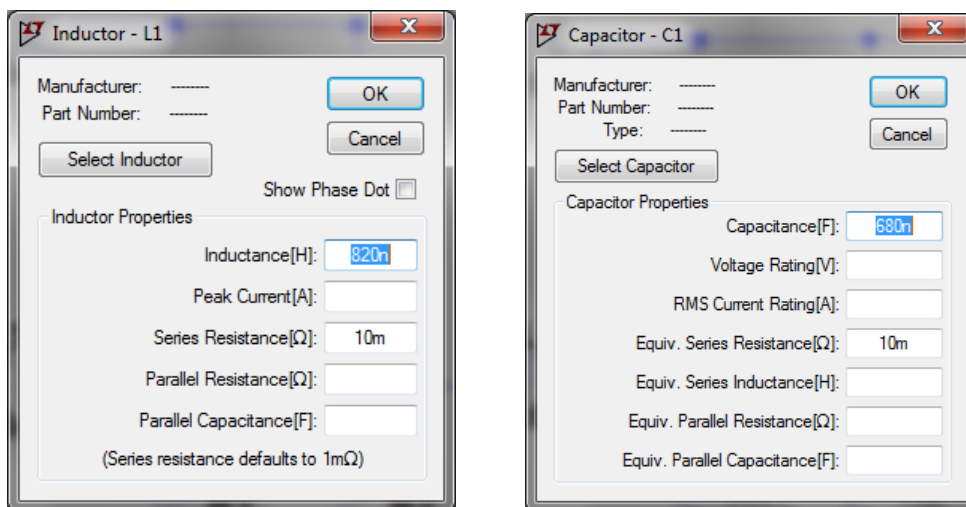
(a) Inductor

(b) Capacitor

Figure A.3: Additional Small Resistance

At last, when using ideal component in the model, there might be pure LC loop in the circuit, which could cause some problems during the simulation as well. To solve this, a small series resistance is needed in the inductor and the capacitor as presented in Figure A.3.